UNIVERSITY OF BELGRADE
FACULTY OF PHYSICS

MASTER THESIS

Quantum Droplets in Dipolar Ring-shaped Bose-Einstein Condensates

---

Author:
Marija Šindik

Supervisor:
Dr. Antun Balaž

September, 2020

UNIVERZITET U BEOGRADU
FIZIČKI FAKULTET

MASTER TEZA

Kvantne kapljice u dipolnim prstenastim Boze-Ajnštajn kondenzatima

---

Autor:
Marija Šindik

Mentor:
Dr Antun Balaž

Septembar, 2020.

Acknowledgments

I would like to express my sincerest gratitude to my advisor Dr. Antun Balaž, for his guidance, patience, useful suggestions and for the time and effort he invested in the making of this thesis.

I would also like to thank my family and friends for the emotional support and encouragement.

This thesis is written in the Scientific Computing Laboratory, Center for the Study of Complex Systems of the Institute of Physics Belgrade. Numerical simulations were run on the PARADOX supercomputing facility at the Scientific Computing Laboratory of the Institute of Physics Belgrade.

Contents

Chapter 1

Introduction

Bose-Einstein condensation as a concept was established theoretically in 1924, when Albert Einstein, following the work of Satyendra Nath Bose [1] on the statistics of photons, predicted a phase transition in a gas of noninteracting bosons (particles with integer spin) [2]. This phase transition occurs at a certain temperature, and is characterized by the macroscopic occupation of the system's ground state. At first it was believed that this concept is purely theoretical, and that the phenomenon will not be practically realized in the presence of even the smallest interactions. However, after the discovery of superfluidity in liquid helium in 1938 [3, 4], it was suggested that there is a connection between those two effects [5], and intensive theoretical research was aimed at the description of interacting Bose gasses, as well as the relationship between Bose-Einstein condensation and superfluidity. The first experimental realization of a Bose-Einstein condensate (BEC) came 70 years after its prediction, since there was a need for developing advanced cooling techniques in order to achieve temperatures low enough, such that the effect occurs. BECs were first obtained in experiments in 1995, using ultracold vapors of rubidium [6], sodium [7], and soon after in lithium [8].

The theoretical description of Bose condensation is centered around the Gross-Pitaevskii equation, derived in 1961. This equation describes weakly interacting dilute Bose gas at low temperatures, and represents the mean-field description of the system [9, 10]. It relies on the approximation of complex van der Waals forces by the pseudo-potential, which leads to the description of these interactions by a single parameter, the s-wave scattering length a_s. The extension of the description to beyond-mean-field effects was derived by Lee, Huang and Yang (LHY) in 1957 [11], based on the Bogoliubov description of elementary excitations [12]. They derived corrections to the chemical potential and condensate depletion, which exist as a consequence of quantum fluctuations due to the contact interaction, and do not vanish even at zero temperature.

The first experimental realization of a BEC in dipolar gases was performed in 2005 with chromium atoms [13], which posses a small permanent magnetic dipole moment. Shortly afterwards, this was also accomplished for magnetic atoms with stronger dipole moments, such as dysprosium [14, 15] and erbium [16]. This opened up a possibility of

exploring the effects of the dipole-dipole interaction (DDI) in BECs [17, 18], which is of significant interest because the DDI is long ranged, in contrast to the short-ranged contact interaction. Additionally, the DDI strongly depends on the relative position of dipoles, which determines whether it is attractive or repulsive, while the contact interaction can only be either one of those, depending on the sign of a_s. Furthermore, using Feshbach resonances [19], the strength of the contact interaction can be tuned to arbitrary values, including the small ones, via the external magnetic field, thus emphasizing the dipolar effects even more.

A system of confined dipoles is usually metastable, and its stability can be achieved only if a strong enough repulsive contact interaction is present, to resist the collapse of the system due to the attractive part of the DDI [20]. Geometry of the system (trap) plays a significant role here, and therefore experiments often use restricted topologies, such as quasi-1D (cigar-shaped) or quasi-2D (pancake-shaped). At low temperatures, the corrections to the system behaviour due to quantum and thermal fluctuations are usually considered negligible. However, a system that is expected to collapse according to the mean-field description, in some cases can be stabilized due to quantum fluctuations, since the LHY term can be effectively repulsive. In order for this to happen, we need to have competing interactions, one attractive and one repulsive, which cancel out at the mean-field level, leaving quantum fluctuations to adjudicate the fate of the system. This is precisely what happens in systems with the strong DDI and repulsive contact interaction. A stable state created in this way, in which there is a competition between the interactions at the mean-field level, and whose stability is saved by the LHY repulsive quantum fluctuation terms, is called a quantum droplet [21, 22]. A quantum droplet is self-bound state [23], surviving for considerable amount of time even after the bounding trap potential is switched off. A density of the droplet still has very low values (eight orders of magnitude lower than that of liquid helium droplets), and meets the diluteness condition. However, it is at least one order of magnitude higher than the density of a BEC and can be considered a quantum liquid, since it is practically incompressible [24, 25].

The aim of this thesis is to numerically investigate the regime in which a quantum droplet can be formed in dipolar condensates. Additionally, we investigate the topology effects by considering the system confined in a ring-shaped potential, that imposes a geometric constraint on the spatial distribution of the resulting droplets, making the system effectively one-dimensional with periodic boundary conditions.

In Chapter 2 we describe basic theoretical principles governing the behavior of dilute weakly-interacting dipolar Bose-Einstein condensates. We give the mean-field description of the system, as well as corrections due to quantum fluctuations induced by the contact and dipole-dipole interaction. In Chapter 3 we present the main features of the used numerical algorithm, based on the split-step Crank-Nicolson method for solving nonlinear differential equations of the dipolar Gross-Pitaevskii type. We present and discuss our numerical results of numerical simulations in Chapter 4, while Chapter 5 summarizes our conclusions.

Chapter 2

Theoretical description of ultracold Bose gases

In this section we describe the basic theoretical principles governing the behavior of dipolar Bose-Einstein condensates, as well as explain the methods for deriving dynamical equations that are later used for numerical simulations. Although Bose-Einstein condensation can theoretically be studied for an ideal gas, in reality there are always some interactions present between atoms or molecules that make up the system under consideration, and they are actually very important to experimentally achieve the condensation. Nonlinearities of equations caused by the interactions are what yields a plethora of new phenomena, such as solitons [26], vortices [27], striped states [28], density oscillations [29], etc.

The system we study is a dilute bosonic gas consisting of N particles in a box of volume Ω. The temperature of the system is considered to be very low, so that the BEC can be produced, and the interactions between atoms are considered to be weak and repulsive. For such a system, it can be shown that complex van der Waals interactions between particles can be approximated by an effective contact interaction, up to measurement errors of observable physical properties. For a gas of magnetic or electric dipolar particles, another type of interaction is present, a dipole-dipole interaction, which can be controlled by an external magnetic or electric field. In the mean-field approximation, an equation describing such systems is known as the Gross-Pitaevskii equation [9, 10]. However, considering beyond-mean-field effects, it is well known that quantum fluctuations emerge, and cause a decrease in the number of particles in the condensate (condensate depletion), even at zero temperature [11]. Precisely this is the main mechanism that enables stabilization of otherwise unstable dipolar BECs and emergence of quantum droplets, a new state of matter, that are a key subject of this thesis [24, 25].

2.1 Contact interaction

The interactions between atoms are an important factor to experimentally achieve Bose-Einstein condensation. The temperatures reached by Zeeman slowers and laser cooling are insufficiently low to produce a BEC (at the experimentally realizable densities), thus the technique of evaporative cooling is used as the final stage. The process involves opening up (reducing the height) of the magneto-optical trap that confines the system, which causes the fastest, and hence the highest-energy atoms to escape from the trap. The remaining sample is left in a non-equilibrium state. It is the interactions between atoms that lead to re-equilibration, through scattering and exchange of energy and momentum. The system eventually reaches an equilibrium state with lower temperature [10].

The important point here is that in dilute gases the range of interatomic forces is much smaller than the average distance between the particles [30]. Hence, only two-body interactions give significant contribution, whereas three- and higher-body interactions can be safely neglected.

To describe two-body scatterings, we consider the wave function for the relative motion of two particles at large distances, since we are not interested in the events at small length scales. This wave function can be written in the form

$$\psi(\boldsymbol{r}) = e^{ikz} + f(\theta)\frac{e^{ikr}}{r}, \tag{2.1}$$

where the first term corresponds to the incoming plane wave along the z direction, and the second term to the outgoing spherical wave. The function $f(\theta)$ is called the *scattering amplitude*, and for the central potential considered here, it can be shown to depend only on the scattering angle θ, which is the angle between the directions of the relative momentum before and after scattering.

In the limit of very low energies, it can be shown that the scattering amplitude approaches a constant value, independent of energy E and the scattering angle θ [9],

$$f(\theta)_{E\to 0} = -a_s. \tag{2.2}$$

The quantity a_s is called the *s-wave scattering length*, and can be interpreted as the minimal distance to which the particles approach each other.

This implies that for a dilute, low-energy gas, it is sufficient to consider only the s-wave scattering, and all the macroscopic properties of the system depend only on the scattering length and not on the details of the interatomic potential. In other words, two interatomic potentials, corresponding to the same scattering length, lead to the same properties of the condensed gas.

Using the Born approximation, the scattering length for two identical particles is given by

$$a_s = \frac{m}{4\pi\hbar^2}\int V(\boldsymbol{r})d\boldsymbol{r}, \tag{2.3}$$

where m is the mass of an atom, $\hbar$ is the reduced Planck's constant, and $V(\boldsymbol{r})$ is the interatomic potential, which can be replaced by an effective (pseudo-) potential giving

the same physical behavior for the same scattering length a_s. The simplest interaction between two particles at points $\boldsymbol{r}$ and $\boldsymbol{r}'$ is the contact interaction, given by

$$V_{\text{eff}}(\boldsymbol{r}, \boldsymbol{r}') = g\delta(\boldsymbol{r} - \boldsymbol{r}'), \tag{2.4}$$

where $g = 4\pi\hbar^2 a_s/m$ is the *contact interaction strength* (sometimes also called *nonlinearity*), and δ denotes the Dirac delta function.

For positive values of the scattering length a_s the interaction is effectively repulsive, while for negative values of a_s it is attractive. In an experiment it is possible to change the value in the range of several orders of magnitude, and even the sign of the scattering length, by changing the strength of an external magnetic field. This is a consequence of the appearance of Feshbach resonances, and makes ultracold atomic systems extremely tunable and versatile [19].

2.2 The Gross-Pitaevskii equation

2.2.1 The field operator

Let us now consider a system of a dilute Bose gas at low temperatures in an external potential $U(\boldsymbol{r})$, with the two-body interaction potential $V(\boldsymbol{r} - \boldsymbol{r}')$. We assume that the interatomic potential depends only on the relative position of the atoms, which is usually the case. The Hamiltonian of the system in a coordinate representation can be written as follows [9]

$$\hat{H} = \sum_i \left(-\frac{\hbar^2}{2m}\nabla_i^2 + U(\boldsymbol{r_i}) \right) + \frac{1}{2}\sum_{i \neq j} V(\boldsymbol{r_i} - \boldsymbol{r_j}). \tag{2.5}$$

The sums in the above equation go over all particles in the system. In the language of second quantization, the Hamiltonian takes the following form

$$\begin{aligned} \hat{H} = &\int d\boldsymbol{r} \left(\frac{\hbar^2}{2m}\nabla\hat{\Psi}^\dagger(\boldsymbol{r})\nabla\hat{\Psi}(\boldsymbol{r}) \right) + \int d\boldsymbol{r}\, U(\boldsymbol{r})\hat{\Psi}^\dagger(\boldsymbol{r})\hat{\Psi}(\boldsymbol{r}) \\ &+ \frac{1}{2}\iint d\boldsymbol{r}\, d\boldsymbol{r}'\hat{\Psi}^\dagger(\boldsymbol{r})\hat{\Psi}^\dagger(\boldsymbol{r}')V(\boldsymbol{r} - \boldsymbol{r}')\hat{\Psi}(\boldsymbol{r}')\hat{\Psi}(\boldsymbol{r}), \end{aligned} \tag{2.6}$$

where $\hat{\Psi}^\dagger(\boldsymbol{r})$ $\left(\hat{\Psi}(\boldsymbol{r})\right)$ is the field operator creating (annihilating) a particle at point $\boldsymbol{r}$, and the integration goes over the entire space. The field operators satisfy the well-known bosonic commutation relations

$$\begin{aligned} \left[\hat{\Psi}(\boldsymbol{r}), \hat{\Psi}^\dagger(\boldsymbol{r}')\right] &= \delta(\boldsymbol{r} - \boldsymbol{r}'), \\ \left[\hat{\Psi}^\dagger(\boldsymbol{r}), \hat{\Psi}^\dagger(\boldsymbol{r}')\right] &= \left[\hat{\Psi}(\boldsymbol{r}), \hat{\Psi}(\boldsymbol{r}')\right] = 0. \end{aligned} \tag{2.7}$$

They are used to define the density of the system

$$n(\boldsymbol{r}) = \langle\hat{\Psi}^\dagger(\boldsymbol{r})\hat{\Psi}(\boldsymbol{r})\rangle, \tag{2.8}$$

where $\langle ... \rangle$ denotes the statistical averaging over all degrees of freedom in the system.

The field operators in the Schrödinger picture depend also on time, and their evolution is governed by the Heisenberg equation

$$i\hbar \frac{\partial}{\partial t} \hat{\Psi}(\boldsymbol{r}, t) = \left[\hat{\Psi}(\boldsymbol{r}, t), \hat{H} \right]. \tag{2.9}$$

Inserting Eq. (2.6) into Eq. (2.9) and using the commutation relations for the field operators (2.7), the following equation for the evolution of the field operator is obtained

$$i\hbar \frac{\partial}{\partial t} \hat{\Psi}(\boldsymbol{r}, t) = \left[-\frac{\hbar^2}{2m} \Delta + U(\boldsymbol{r}, t) + \int d\boldsymbol{r}' \hat{\Psi}^\dagger(\boldsymbol{r}', t) V(\boldsymbol{r} - \boldsymbol{r}') \hat{\Psi}(\boldsymbol{r}', t) \right] \hat{\Psi}(\boldsymbol{r}, t). \tag{2.10}$$

As is discussed in the previous section, the actual form of the interatomic potential is not important for the calculation of relevant properties of a dilute, low-temperature gas, as long as the potential produces the correct value for the scattering length. We are therefore allowed to replace the exact interatomic potential with the effective potential given by Eq. (2.4).

2.2.2 The Bogoliubov approximation

Another important approximation that needs to be carried out is associating the field operator $\hat{\Psi}(\boldsymbol{r}, t)$ with the classical field (wave-function) $\Psi(\boldsymbol{r}, t)$. For a uniform system occupying a volume Ω, the field operator can be expressed in a basis of plane waves according to the formula

$$\hat{\Psi}(\boldsymbol{r}) = \sum_{\boldsymbol{p}} \frac{1}{\sqrt{\Omega}} e^{i\boldsymbol{p}\cdot\boldsymbol{r}/\hbar} \hat{a}_{\boldsymbol{p}}. \tag{2.11}$$

The quantity $\hat{a}_{\boldsymbol{p}}$ is the annihilation operator that destroys a particle in a state with momentum $\boldsymbol{p}$. The spectrum of momenta in the above sum is determined by the boundary conditions. For a truly homogeneous system in infinite space all momenta are present. A similar equation holds for the creation operators. It can be derived that the operators $\hat{a}^\dagger_{\boldsymbol{p}}$ and $\hat{a}_{\boldsymbol{p}}$ also satisfy the bosonic commutation relations similar to those given by Eq. (2.7),

$$\left[\hat{a}_{\boldsymbol{p}}, \hat{a}^\dagger_{\boldsymbol{p}'} \right] = \delta_{\boldsymbol{p},\boldsymbol{p}'}, \quad \left[\hat{a}^\dagger_{\boldsymbol{p}}, \hat{a}^\dagger_{\boldsymbol{p}'} \right] = \left[\hat{a}_{\boldsymbol{p}}, \hat{a}_{\boldsymbol{p}'} \right] = 0, \tag{2.12}$$

where $\delta_{\boldsymbol{p},\boldsymbol{p}'}$ is a Kronecker delta function.

At very low temperatures, when the BEC phase is present, the occupation N_0 of a state with $\boldsymbol{p} = 0$, i.e., the state with the lowest energy, is significantly higher than for any other state, and corresponds to a macroscopic occupation of the ground state. Therefore, it is useful to decompose the field operator into a condensate and a thermal (non-condensed) part,

$$\hat{\Psi}(\boldsymbol{r}) = \frac{1}{\sqrt{\Omega}} \hat{a}_0 + \sum_{\boldsymbol{p} \neq 0} \frac{1}{\sqrt{\Omega}} e^{i\boldsymbol{p}\cdot\boldsymbol{r}/\hbar} \hat{a}_{\boldsymbol{p}}. \tag{2.13}$$

We now introduce the Bogoliubov approximation, which consists of replacing the operators $\hat{a}_0$ and $\hat{a}^\dagger_0$ with the c-number $\sqrt{N_0}$. This is motivated by the fact that $\langle \hat{a}^\dagger_{\boldsymbol{0}} \hat{a}_{\boldsymbol{0}} \rangle = N_0$,

and is equivalent to treating the first part of the field operator in Eq. (2.13) as a classical field,

$$\hat{\Psi}(\boldsymbol{r}) = \Psi_0(\boldsymbol{r}) + \delta\hat{\Psi}(\boldsymbol{r}). \tag{2.14}$$

The function $\Psi_0(\boldsymbol{r})$ is called the wave function of the condensate, while the second term corresponds to quantum fluctuations.

To the lowest order, which is usually called the *mean-field theory*, at very low temperatures one can simply replace the operator $\hat{\Psi}(\boldsymbol{r})$ in Eq. (2.10) with a classical field $\Psi(\boldsymbol{r})$. By replacing the interatomic potential according to Eq. (2.4) one finally obtains the equation

$$i\hbar\frac{\partial}{\partial t}\Psi(\boldsymbol{r},t) = \left(-\frac{\hbar^2}{2m}\Delta + U(\boldsymbol{r},t) + g|\Psi(\boldsymbol{r},t)|^2\right)\Psi(\boldsymbol{r},t). \tag{2.15}$$

This is the time-dependent *Gross-Pitaevskii equation*. The wave function $\Psi(\boldsymbol{r})$ is normalized to the number of particles in a system,

$$\int d\boldsymbol{r}\ |\Psi(\boldsymbol{r})|^2 = N. \tag{2.16}$$

We point out that Eq. (2.15) is essentially a time-dependent Schrödinger equation, with an additional nonlinear term describing the contact interaction.

2.2.3 The time-independent Gross-Pitaevskii equation

Let us go back briefly to the first quantization description of the system, given by Eq. (2.5), with the effective interatomic potential (2.4). In a fully condensed state, all particles are in the same single-particle state $\phi(\boldsymbol{r})$. In the Hartree (mean-field) approximation, the many-body wave function is given as a symmetrized product of single-particle wave functions [10]

$$\Psi(\boldsymbol{r}_1,...,\boldsymbol{r}_N) = \prod_i \phi(\boldsymbol{r}_i). \tag{2.17}$$

This wave function does not take into account the correlations among particles.

The energy of a system in the state Ψ is calculated as the expectation value of the Hamiltonian (2.5) in this state, as follows

$$E = \int d\boldsymbol{r}_1...d\boldsymbol{r}_N\ \Psi^*\hat{H}\Psi = \int d\boldsymbol{r}\ \left(N\frac{\hbar^2}{2m}|\nabla\phi(\boldsymbol{r})|^2 + NU(\boldsymbol{r})|\phi(\boldsymbol{r})|^2 + \frac{N(N-1)}{2}g|\phi(\boldsymbol{r})|^4\right). \tag{2.18}$$

It is convenient to introduce the wave function $\psi(\boldsymbol{r})$ of the condensed state as

$$\psi(\boldsymbol{r}) = \sqrt{N}\phi(\boldsymbol{r})\,, \tag{2.19}$$

in order to satisfy the normalization condition (2.16). The energy of the system can now be written as

$$E = \int d\boldsymbol{r}\ \left(\frac{\hbar^2}{2m}|\nabla\psi(\boldsymbol{r})|^2 + U(\boldsymbol{r})|\psi(\boldsymbol{r})|^2 + \frac{1}{2}g|\psi(\boldsymbol{r})|^4\right)\,, \tag{2.20}$$

where we neglected terms of the order $1/N$. A solution for the wave function can be found by minimizing this energy functional varying $\psi(\boldsymbol{r})$, with the constraint of preserving the normalization, set by the Lagrange multiplier μ. By solving the minimization condition $\delta\left(E-\mu N\right)=0$, we obtain the following expression

$$\mu\,\psi(\boldsymbol{r})=\left(-\frac{\hbar^2}{2m}\nabla^2+U(\boldsymbol{r})+g|\psi(\boldsymbol{r})|^2\right)\psi(\boldsymbol{r}). \tag{2.21}$$

This is the time-independent Gross-Pitaevskii equation. The Lagrange multiplier μ corresponds to the chemical potential and is the eigenvalue of the single-particle Gross-Pitaevskii Hamiltonian,

$$\hat{H}=-\frac{\hbar^2}{2m}\nabla^2+U(\boldsymbol{r})+g|\psi(\boldsymbol{r})|^2\,. \tag{2.22}$$

2.3 Dipole-dipole interaction

We now turn to the description of an additional interaction among atoms, the dipole-dipole interaction (DDI), which is present between atoms or molecules with a non-vanishing magnetic or electric dipole moment. Here we will focus on magnetic systems, since they are readily available in experiments, while electric systems are still under development. In a system with free magnetic dipole moments, their orientation is random, yielding a zero net magnetic moment of the system. However, in the presence of an external magnetic field, the dipole moments will be oriented along the magnetic field, which corresponds to the lowest potential energy of the system. The forces opposing this alignment are thermal in origin, and thus very weak at low temperatures. We can assume that at very low temperatures all magnetic dipoles are oriented along the external magnetic field, which is chosen to coincide with the z axis. Then the interaction potential between two particles with the magnetic dipole moment $\boldsymbol{\mu}$ is given by

$$V_{\mathrm{dd}}(\boldsymbol{r}-\boldsymbol{r}')=\frac{\mu_0\mu^2}{4\pi}\frac{1-3\cos^2\theta}{|\boldsymbol{r}-\boldsymbol{r}'|^3}, \tag{2.23}$$

where μ_0 is the magnetic vacuum permeability, $\boldsymbol{r}$ and $\boldsymbol{r}'$ are positions of two particles, and θ is the angle between the relative position of the particles $\boldsymbol{r}-\boldsymbol{r}'$ and the dipole orientation (z axis).

In contrast to the contact interaction, which is short-ranged and isotropic, the DDI is long-ranged and anisotropic. It strongly depends on the relative positions of the two dipoles, and can be both attractive and repulsive, depending on the angle θ. For example, two dipoles that are on top of each other (head-to-tail configuration) will have an attractive interaction, whereas two dipoles next to each other (side-by-side configuration) will repel. The DDI will cause the system to be stretched along the axis of an external magnetic field, i.e., along the orientation of the dipoles.

The DDI strength is usually defined by the dipolar length

$$a_{\mathrm{dd}}=\frac{\mu_0\mu^2 m}{12\pi\hbar^2}, \tag{2.24}$$

which is a convenient measure and can be used to compare the strength of the DDI and the contact interaction, whose strength is expressed in terms of the s-wave scattering length.

For a positive scattering length $a_s > 0$, the contact interaction is always repulsive and the system is unconditionally stable. However, in the presence of dipole-dipole interactions, depending on the geometry, the system can collapse if the number of particles is large enough, or the dipole moment of the particles is sufficiently large [20].

2.4 Beyond-mean-field approximation

The mean-field approximation described in Sec. 2.2.2 that consist of replacing the field operator by the classical field, does not take into account effects of thermal and quantum fluctuations described by the second term in Eq. (2.14). Assuming that we are at zero temperature, the fluctuations term stems from the presence of interactions, which can expel particles from the ground state into excited states, even at zero temperature. For now, we are considering a homogeneous gas of bosonic particles (when the external trap potential is absent), as a starting point to describing trapped systems that are commonly realized in experiments. Taking into account quantum fluctuations leads to beyond-mean-field theory.

2.4.1 Fluctuations due to the contact interaction

In order to investigate fluctuations, it is convenient to look at the Hamiltonian in the momentum basis. For now, let us limit our discussion only to the contact interaction. The substitution of Eq. (2.11) into Eq. (2.6), while neglecting the external potential, gives the following expression for the Hamiltonian [9]

$$\hat{H} = \sum_{\boldsymbol{p}} \frac{p^2}{2m} \hat{a}^\dagger_{\boldsymbol{p}} \hat{a}_{\boldsymbol{p}} + \frac{1}{2\Omega} \sum_{\boldsymbol{p}_1, \boldsymbol{p}_2, \boldsymbol{q}} V_{\boldsymbol{q}} \hat{a}^\dagger_{\boldsymbol{p}_1+\boldsymbol{q}} \hat{a}^\dagger_{\boldsymbol{p}_2-\boldsymbol{q}} \hat{a}_{\boldsymbol{p}_1} \hat{a}_{\boldsymbol{p}_2}. \tag{2.25}$$

The quantity $V_{\boldsymbol{q}}$ represents the Fourier transform of the interaction potential $V(\boldsymbol{r})$, defined as

$$V_{\boldsymbol{q}} = \int d\boldsymbol{r}\, e^{-i\boldsymbol{q}\cdot\boldsymbol{r}/\hbar} V(\boldsymbol{r}). \tag{2.26}$$

The first term in the Hamiltonian (2.25) corresponds to the kinetic energy of the system, expressed as a sum over all momenta, where kinetic energy of a particle in a state with momentum $\boldsymbol{p}$ is multiplied by the number of particles in that state. The second term describes the contact interaction energy, as a sum of all possible scattering processes in which two particles with momenta $\boldsymbol{p}_1$ and $\boldsymbol{p}_2$ exchange the momentum $\boldsymbol{q}$ due to the presence of the two-body interaction $V_{\boldsymbol{q}}$.

Since only small momenta are relevant at low temperatures, we are allowed to consider only the $\boldsymbol{q} = 0$ value of $V_{\boldsymbol{q}}$. The mean-field approximation is equivalent to neglecting all the terms containing the operators $\hat{a}_{\boldsymbol{p}}$ and $\hat{a}^\dagger_{\boldsymbol{p}}$ with $\boldsymbol{p} \neq 0$. However, to take into

account the fluctuations to lowest order, we need to retain the terms up to second order in particle operators with $\boldsymbol{p} \neq 0$. This yields the Hamiltonian

$$\hat{H} = \sum_{\boldsymbol{p}} \frac{p^2}{2m} \hat{a}^\dagger_{\boldsymbol{p}} \hat{a}_{\boldsymbol{p}} + \frac{V_0}{2\Omega} \hat{a}^\dagger_0 \hat{a}^\dagger_0 \hat{a}_0 \hat{a}_0 + \frac{V_0}{2\Omega} \sum_{\boldsymbol{p}\neq 0} \left(4\hat{a}^\dagger_0 \hat{a}^\dagger_{\boldsymbol{p}} \hat{a}_0 \hat{a}_{\boldsymbol{p}} + \hat{a}^\dagger_0 \hat{a}^\dagger_0 \hat{a}_{\boldsymbol{p}} \hat{a}_{-\boldsymbol{p}} + \hat{a}^\dagger_{\boldsymbol{p}} \hat{a}^\dagger_{-\boldsymbol{p}} \hat{a}_0 \hat{a}_0 \right). \quad (2.27)$$

In the Bogoliubov approximation, we replace operators $\hat{a}_0$ and $\hat{a}^\dagger_0$ by $\sqrt{N_0}$. Since the number of particles in excited states is very small, $N \approx N_0$, and we can replace operators $\hat{a}_0$ and $\hat{a}^\dagger_0$ in the third term of Eq. (2.27) by $\sqrt{N}$. However, in the second term we have to be more careful and to work with higher accuracy by using the normalization relation

$$\hat{a}^\dagger_0 \hat{a}_0 + \sum_{\boldsymbol{p}\neq 0} \hat{a}^\dagger_{\boldsymbol{p}} \hat{a}_{\boldsymbol{p}} = N. \quad (2.28)$$

By neglecting the higher-order terms, we obtain

$$\hat{a}^\dagger_0 \hat{a}^\dagger_0 \hat{a}_0 \hat{a}_0 = N^2 - 2N \sum_{\boldsymbol{p}\neq 0} \hat{a}^\dagger_{\boldsymbol{p}} \hat{a}_{\boldsymbol{p}}. \quad (2.29)$$

As for the Fourier transform of the contact interaction, in the lowest-order Born approximation it simply reduces to $V_0 = g$, where g is the earlier introduced contact interaction strength. Analogously, we have to employ higher-order perturbation theory to find the first correction to the effective potential. It can be shown that, after this correction is calculated, the renormalized contact interaction has the following form

$$V_0 = g\left(1 + \frac{g}{\Omega} \sum_{\boldsymbol{p}\neq 0} \frac{m}{p^2}\right). \quad (2.30)$$

Substituting Eq. (2.29) and Eq. (2.30) into Eq. (2.27), and neglecting the higher-order terms, we get the following expression for the Hamiltonian

$$\hat{H} = \sum_{\boldsymbol{p}} \frac{p^2}{2m} \hat{a}^\dagger_{\boldsymbol{p}} \hat{a}_{\boldsymbol{p}} + \frac{gN^2}{2\Omega} + \frac{gn}{2} \sum_{\boldsymbol{p}\neq 0} \left(2\hat{a}^\dagger_{\boldsymbol{p}} \hat{a}_{\boldsymbol{p}} + \hat{a}^\dagger_{\boldsymbol{p}} \hat{a}^\dagger_{-\boldsymbol{p}} + \hat{a}_{\boldsymbol{p}} \hat{a}_{-\boldsymbol{p}} + \frac{mgn}{p^2} \right), \quad (2.31)$$

where $n = N/\Omega$ is the density of the gas.

The Hamiltonian (2.31) is not in the diagonal form, since it contains terms $\hat{a}^\dagger_{\boldsymbol{p}} \hat{a}^\dagger_{-\boldsymbol{p}}$ and $\hat{a}_{\boldsymbol{p}} \hat{a}_{-\boldsymbol{p}}$. It can be diagonalized by introducing a new set of operators $\hat{b}_{\boldsymbol{p}}$ and $\hat{b}^\dagger_{\boldsymbol{p}}$ by a linear transformation

$$\begin{aligned} \hat{a}_{\boldsymbol{p}} &= u_{\boldsymbol{p}}\, \hat{b}_{\boldsymbol{p}} + v^*_{-\boldsymbol{p}}\, \hat{b}^\dagger_{-\boldsymbol{p}}, \\ \hat{a}^\dagger_{\boldsymbol{p}} &= u^*_{\boldsymbol{p}}\, \hat{b}^\dagger_{\boldsymbol{p}} + v_{-\boldsymbol{p}}\, \hat{b}_{-\boldsymbol{p}}, \end{aligned} \quad (2.32)$$

which is known as the *Bogoliubov transformation* [12]. The new operators $\hat{b}_{\boldsymbol{p}}$ and $\hat{b}^\dagger_{\boldsymbol{p}}$ represent the annihilation and creation operators of quasi-particles to an excited state, and not of original particles with momentum $\boldsymbol{p}$, as is the case with $\hat{a}_{\boldsymbol{p}}$ and $\hat{a}^\dagger_{\boldsymbol{p}}$.

The coefficients $u_{\boldsymbol{p}}$ and $v_{-\boldsymbol{p}}$ need to be chosen so that the Hamiltonian (2.31) is properly diagonalized, which translates into two conditions. The first one is that $\hat{b}_{\boldsymbol{p}}$ and $\hat{b}^\dagger_{\boldsymbol{p}}$ satisfy the bosonic commutation relations given by the Eq. (2.12), and the second one is that the coefficients of the non-diagonal terms $\hat{b}^\dagger_{\boldsymbol{p}}\hat{b}^\dagger_{-\boldsymbol{p}}$ and $\hat{b}_{\boldsymbol{p}}\hat{b}_{-\boldsymbol{p}}$ in the Hamiltonian (2.31) vanish. After a simple calculation, it can be shown that these two conditions yield the following result for the coefficients $u_{\boldsymbol{p}}$ and $v_{-\boldsymbol{p}}$:

$$u_{\boldsymbol{p}}, v_{-\boldsymbol{p}} = \pm\left(\frac{p^2/2m + gn}{2\epsilon(p)} \pm \frac{1}{2}\right)^{1/2}, \tag{2.33}$$

where the energy dispersion function $\epsilon(p)$ is defined below in Eq. (2.36).

The Hamiltonian is now given in the diagonal form,

$$\hat{H} = E_0 + \sum_{\boldsymbol{p}} \epsilon(p)\, \hat{b}^\dagger_{\boldsymbol{p}}\, \hat{b}_{\boldsymbol{p}}, \tag{2.34}$$

where E_0 is the ground state energy given by the expression

$$E_0 = g\frac{N^2}{2\Omega} + \frac{1}{2}\sum_{\boldsymbol{p}\neq 0}\left(\epsilon(p) - gn - \frac{p^2}{2m} + \frac{mg^2n^2}{p^2}\right), \tag{2.35}$$

and $\epsilon(p)$ is the energy of elementary excitations,

$$\epsilon(p) = \sqrt{\frac{gn}{m}p^2 + \left(\frac{p^2}{2m}\right)^2}. \tag{2.36}$$

Equation (2.36) represents the Bogoliubov dispersion law for elementary excitations of the system. In the low-momentum limit the Bogoliubov dispersion becomes linear, giving rise to phonon-like excitations, which are responsible for the superfluidity of the system.

The ground state energy can be calculated by replacing the sum with an integral in momentum space in Eq. (2.35), which yields the following expression

$$E_0 = gnN\left(1 + \frac{32}{3}\sqrt{\frac{na_s^3}{\pi}}\right). \tag{2.37}$$

This result is called the Lee-Huang-Yang (LHY) expansion [11]. The first term represents the ground state energy of a system in the mean-field approximation, while the second term corresponds to corrections due to fluctuations. The chemical potential can be easily calculated using the relation $\mu = \partial E_0/\partial N$, yielding

$$\mu = gn\left(1 + \frac{32}{3}\sqrt{\frac{na_s^3}{\pi}}\right). \tag{2.38}$$

Another set of important quantities are particle occupation numbers $n_{\boldsymbol{p}}$. Using the introduced Bogoliubov transformations (2.32), one easily find

$$n_{\boldsymbol{p}} = \langle \hat{a}^\dagger_{\boldsymbol{p}} \hat{a}_{\boldsymbol{p}} \rangle = |v_{-\boldsymbol{p}}|^2 + |u_{\boldsymbol{p}}|^2 \langle \hat{b}^\dagger_{\boldsymbol{p}} \hat{b}_{\boldsymbol{p}} \rangle + |v_{-\boldsymbol{p}}|^2 \langle \hat{b}^\dagger_{-\boldsymbol{p}} \hat{b}_{-\boldsymbol{p}} \rangle. \tag{2.39}$$

We immediately notice that even at zero temperature, when the occupation of excited states is zero, $\langle \hat{b}^\dagger_{\boldsymbol{p}} \hat{b}_{\boldsymbol{p}} \rangle = 0$, there are still particles with non-zero momentum present in the system, the effect known as *quantum fluctuations*.

The density of the condensate at zero temperature can be calculated as

$$n_0 = n - \frac{1}{(2\pi\hbar)^3} \int n_{\boldsymbol{p}} \, d\boldsymbol{p} = n \left(1 - \frac{8}{3} \sqrt{\frac{n a_s^3}{\pi}} \right). \tag{2.40}$$

The phenomenon that not all particles are in the condensed state at zero temperature is called the *condensate depletion*. We note that all the correction terms are described by the square root of the gas parameter $\sqrt{n a_s^3}$, which is guaranteed to be very small compared to 1 if the diluteness condition holds.

2.4.2 Fluctuations due to the dipole-dipole interaction

In previous section we described the effects of quantum fluctuations that emerge from the presence of contact interactions. An analogous calculation can be performed for the DDI. The calculation is quite complicated due to its anisotropic nature, so we show only the final results here. For more details, see Ref. [31, 32].

Taking into account both types of interactions, the corrections for the condensate density and the chemical potential are given by

$$\Delta n = \frac{8}{3} n \sqrt{\frac{n a_s^3}{\pi}} \, Q_3(\epsilon_{\mathrm{dd}}), \tag{2.41}$$

$$\Delta \mu = \frac{32}{3} g n \sqrt{\frac{n a_s^3}{\pi}} \, Q_5(\epsilon_{\mathrm{dd}}), \tag{2.42}$$

where the parameter $\epsilon_{\mathrm{dd}} = a_{\mathrm{dd}}/a_{\mathrm{s}}$ is the relative interaction strength of the DDI with respect to the contact interaction. The functions $Q_l(x)$ represent the integrals

$$Q_l(x) = \int_0^1 du \, (1 - x + 3xu^2)^{l/2}. \tag{2.43}$$

The functions $Q_3(x)$ and $Q_5(x)$ are monotonically increasing when ϵ_{dd} increases from 0 to 1, and for $\epsilon_{\mathrm{dd}} = 0$, the usual results, (2.38) and (2.40), are recovered.

Finally, by putting together all of the above elements, we are able to construct an effective Gross-Pitaevskii equation, that includes the contact and the DDI, as well as corrections due to quantum fluctuations:

$$i\hbar \frac{\partial \Psi(\boldsymbol{r}, t)}{\partial t} = \left[-\frac{\hbar^2}{2m} \Delta + U(\boldsymbol{r}) + g n(\boldsymbol{r}, t) + \int d\boldsymbol{r}' \, V(\boldsymbol{r} - \boldsymbol{r}') n(\boldsymbol{r}', t) + \Delta\mu \right] \Psi(\boldsymbol{r}, t). \tag{2.44}$$

Here $n(\boldsymbol{r},t)$ is the total density of particles,

$$n(\boldsymbol{r},t) = n_0(\boldsymbol{r},t) + \triangle n, \tag{2.45}$$

where $n_0(\boldsymbol{r},t) = |\Psi(\boldsymbol{r},t)|^2$ is the condensate density, and the condensate depletion $\triangle n$ is given by Eq. (2.41). The condition of preserving the total number of particles is now given through the normalization of the total density,

$$\int d\boldsymbol{r}\, n(\boldsymbol{r},t) = N. \tag{2.46}$$

Note that we have also included the trap potential in Eq. (2.44), assuming that the local density approximation is valid. We use the above system of equations throughout this thesis.

2.5 Quantum droplets

The presence of quantum fluctuations in an ultracold dipolar Bose system is equivalent to having an effective additional interaction, that turns out to be repulsive for a positive scattering length, the case we consider. This is due to the fact that the corresponding shift of the chemical potential $\triangle\mu$, which is added to the Hamiltonian, is always positive, while the contribution of the condensate depletion to the DDI term, which can give negative terms, is practically negligible.

In the mean-field approach, the stability of the dipolar Bose system can be achieved if the repulsive contact interaction dominates over the attractive DDI. Alternatively, if the strength of the DDI or the number of particles is large enough, the system may collapse [20]. The effective repulsive interaction due to quantum fluctuations may be able to prevent the collapse of the system for some range of parameter values, when the residual mean-field attractive interaction is small enough. The quantum fluctuations term may become significant for high densities, since it depends on the density as $n^{3/2}$, in comparison with the contact and the dipole-dipole interaction, for which this dependence is linear. As a consequence, the collapse of the system may be avoided on account of an increase in quantum fluctuations, which results in expelling particles from the condensate.

This is the process of quantum stabilization, which yields a stable system consisting of self-bound clusters of atoms, known as *quantum droplets*. Redistribution of particles into a number of individual droplets, instead of remaining in a global condensate, serves as a mechanism of preventing the energy to go to large negative values, i.e., it practically makes it bounded from below. The density of such droplets is at least one order of magnitude higher than the density of a BEC, and therefore they can be thought of as a quantum liquid, which motivated the term droplets. However, it is important to note that the density of the droplets is still several orders of magnitude smaller than for the fluids from everyday life, making the diluteness condition still satisfied.

Quantum droplets can be formed as a result of the interplay between the long-range DDI and the short-range contact interaction described above, by preparing a system in a

stable BEC phase, and then reducing the strength of the contact interaction by a sudden quench [22]. But this is not a unique experimental protocol for realizing the droplets. Another scenario for creating quantum droplets relies on tilting of the orientation of the dipoles (by tilting the external magnetic field) [33]. The droplets may be created even when there is only a short-range contact interaction in the system, but this requires at least a two-component BEC [34]. Here it is necessary for the two components to attract each other and in this way provide a source of instability, which is then balanced by the repulsive intra-component interactions and quantum fluctuations.

Chapter 3

Numerical methods

The effective Gross-Pitaevskii (GP) equation is a nonlinear differential equation. As opposed to linear differential equations, which can generally always be solved, nonlinear equations are difficult to deal with. If there is no specific analytic method for solving a particular type of nonlinear equations, one has to apply one of various numerical approximative methods.

In this thesis we numerically solve the effective GP equation presented in previous chapter. The numerical method that is used is split-step semi-implicit Crank-Nicolson method. We have used programs that are developed earlier for solving the mean-field dipolar GP equation, and described in detail in Ref. [35–37]. These programs are written in C programming language, and are paralelized using OpenMP and MPI, since the simulations for three-dimensional (3D) systems are computationally very demanding. We have modified the programs to take into account quantum fluctuations and condensate depletion, as detailed in Sec. 2.4. Here we briefly describe the main steps of the algorithm used.

3.1 Rescaling of the effective GP equation

The system of equations that we work with is given by Eq. (2.41) - (2.46). The system is confined to a ring-shaped potential given by

$$U(\boldsymbol{r}) = \frac{1}{2}m\left[\omega_\rho^2\left(\rho - R\right)^2 + \omega_z^2 z^2\right], \tag{3.1}$$

where $\rho = \sqrt{x^2 + y^2}$ is the radial distance, R is the radius of the ring (i.e., radial distance at which the potential is minimal), and ω_ρ and ω_z are the corresponding trap frequencies. This potential is essentially a modified harmonic potential. The external magnetic field, which is responsible for the orientation of the dipole momenta, is assumed to be oriented along the z axis, so the system possesses cylindrical symmetry.

Before proceeding with numerical calculations, we need to convert Eq. 2.44 into a dimensionless form. This can be done by choosing a reference quantity for each variable.

First, we choose a reference frequency $\omega_{\rm ref}$ and express the trap frequencies as

$$\omega_\rho = \eta\omega_{\rm ref}, \quad \omega_z = \lambda\omega_{\rm ref}, \tag{3.2}$$

where η and λ are dimensionless quantities that now define the trap and are used in the programs. It is convenient to choose one of the trap frequencies as the reference one, and usually the largest one is selected. For a reference time we choose $2/\omega_{\rm ref}$, so that the time is written as $t = 2\tilde{t}/\omega_{\rm ref}$, where $\tilde{t}$ is a dimensionless quantity. The factor 2 is taken for convenience, to eliminate the coefficient $1/2$ in front of some terms in Eq. (2.44). A reference length is chosen as a harmonic oscillator length for a reference frequency and reads $\ell = \sqrt{\hbar/(m\omega_{\rm ref})}$, and the coordinates are expressed as $x = \tilde{x}\ell$, $y = \tilde{y}\ell$, $z = \tilde{z}\ell$, $\rho = \tilde{\rho}\ell$, where quantities with the tilde sign are dimensionless. The same rescaling is for all lengths that are used in equations, such as a_s and $a_{\rm dd}$.

The many-body wave function in the mean-field approach satisfies the normalization condition

$$\int d\boldsymbol{r}\, |\Psi(\boldsymbol{r}, t)|^2 = N. \tag{3.3}$$

In addition to expressing it in a dimensionless form, we further rescale the wave function so that the above integral is equal to 1, which is achieved by

$$\Psi(\boldsymbol{r}, t) = \frac{\tilde{\Psi}(\tilde{\boldsymbol{r}}, \tilde{t})\sqrt{N}}{\ell^{3/2}}. \tag{3.4}$$

Using the above rescaling of relevant physical quantities, we can make the whole system of effective equations dimensionless. The rescaling of the particle density and the shift of the chemical potential are given by

$$\tilde{n}\left(\tilde{\boldsymbol{r}}, \tilde{t}\right) = \left|\tilde{\Psi}\left(\tilde{\boldsymbol{r}}, \tilde{t}\right)\right|^2 + \frac{8}{3}\sqrt{\frac{N}{\pi}\left(\frac{a_s}{\ell}\right)^3}\, Q_3(\epsilon_{\rm dd})\left|\tilde{\Psi}\left(\tilde{\boldsymbol{r}}, \tilde{t}\right)\right|^3, \tag{3.5}$$

$$\Delta\tilde{\mu}\left(\tilde{\boldsymbol{r}}, \tilde{t}\right) = \frac{32}{3}\tilde{g}\sqrt{\frac{N}{\pi}\left(\frac{a_s}{\ell}\right)^3}\, Q_5(\epsilon_{\rm dd})\left|\tilde{\Psi}\left(\tilde{\boldsymbol{r}}, \tilde{t}\right)\right|^3. \tag{3.6}$$

Using these transformations the effective GP equation is cast into the dimensionless form as follows

$$i\,\frac{\partial\tilde{\Psi}\left(\tilde{\boldsymbol{r}}, \tilde{t}\right)}{\partial\tilde{t}} = \left[-\tilde{\Delta} + \tilde{U}\left(\tilde{\boldsymbol{r}}\right) + \tilde{g}\tilde{n}\left(\tilde{\boldsymbol{r}}, \tilde{t}\right) + \tilde{g}_{\rm dd}\int d\tilde{\boldsymbol{r}}'\, \tilde{V}_{\rm dd}\left(\tilde{\boldsymbol{r}} - \tilde{\boldsymbol{r}}'\right)\tilde{n}\left(\tilde{\boldsymbol{r}}', \tilde{t}\right) + \Delta\tilde{\mu}\left(\tilde{\boldsymbol{r}}, \tilde{t}\right)\right]\tilde{\Psi}\left(\tilde{\boldsymbol{r}}, \tilde{t}\right), \tag{3.7}$$

where the potentials are given by

$$\tilde{U}\left(\tilde{\boldsymbol{r}}\right) = \eta^2\left(\tilde{\rho} - R/\ell\right)^2 + \lambda^2\tilde{z}^2, \qquad \tilde{V}_{\rm dd}\left(\tilde{\boldsymbol{r}} - \tilde{\boldsymbol{r}}'\right) = \frac{1 - 3\cos^2\theta}{\left|\tilde{\boldsymbol{r}} - \tilde{\boldsymbol{r}}'\right|^3}; \tag{3.8}$$

and the strengths of the contact and dipole-dipole interactions as

$$\tilde{g} = 8\pi N a_s/\ell, \qquad \tilde{g}_{\rm dd} = 6N a_{\rm dd}/\ell. \tag{3.9}$$

The normalization condition in a dimensionless form is

$$\int d\tilde{\boldsymbol{r}}\, \tilde{n}(\tilde{\boldsymbol{r}}, \tilde{t}) = 1. \tag{3.10}$$

3.2 Split-step Crank-Nicolson method

We now briefly describe the numerical method used to solve the system of equations (3.5) - (3.10). For more details and the description of implementation, see Ref. [35].

The method is described on an example of a one-dimensional (1D) equation, considering that generalization to the 3D case is straightforward. The equation that we solve has the following form

$$i\frac{\partial \Psi(x,t)}{\partial t} = \hat{H}\Psi(x,t), \tag{3.11}$$

where $\hat{H}$ stands here for the 1D-equivalent of the Hamiltonian given in Eq. (3.7).

This Hamiltonian can be separated into two parts, $\hat{H} = \hat{H}_1 + \hat{H}_2$, where the first one contains all the terms without spatial derivatives (i.e., the trap and interaction terms), and $\hat{H}_2 = -\Delta$. The propagation of the wave function is then split in two parts (hence the *split-step* part of the method name), corresponding to $\hat{H}_1$ and $\hat{H}_2$ separately,

$$i\frac{\partial \Psi(x,t)}{\partial t} = H_1\Psi(x,t), \tag{3.12}$$

$$i\frac{\partial \Psi(x,t)}{\partial t} = H_2\Psi(x,t). \tag{3.13}$$

This approximation is equivalent to neglecting the noncommutativity of the operators $\hat{H}_1$ and $\hat{H}_2$, since the propagation of the wave function actually happens with respect to $\hat{H}_1 + \hat{H}_2$. We note that the propagation algorithm can be improved to higher orders using the Campbell-Baker-Hausdorff formula, if necessary. However, using the sufficiently small time step for propagation, the corresponding error can be made arbitrarily small, so we rely on the above decomposition.

As usual, the time evolution is divided into N_t time steps of length $\triangle t$. Starting from some initial value of the wave function at time t_0, we first propagate it with respect to H_1 to obtain the intermediate value at $t_0 + \triangle t$. This intermediate solution is then used as an initial value for the propagation with respect to H_2 to obtain the final solution at $t_0 + \triangle t$. This procedure is then repeated $N_t - 1$ times, until the time propagation is finished.

The propagation of the wave function is realized on some finite spatial interval $[-L, L)$, which has a length $2L$ and represents the simulation box. The wave function outside of the box is considered to be sufficiently small, so that it can be set to zero at the simulation box borders. The spatial coordinate is also discretized into a grid of N_x points, $x_k = -L + kh$, where h is the space step (grid spacing) equal to $2L/N_x$, and k goes from 0 to $N_x - 1$. The wave function at grid point x_k and at time $t_n = n\triangle t$ is written, for brevity, as $\Psi(x_k, t_n) = \Psi_k^n$.

To obtain the intermediate solution of the wave function, which we symbolically denote as $\Psi_k^{n+1/2}$, we propagate Ψ_k^n with respect to $\hat{H}_1$. Since this part of the Hamiltonian does not contain any spatial derivatives, the solution can be calculated exactly,

$$\Psi_k^{n+1/2} = e^{-i\triangle t H_{1k}}\, \Psi_k^n, \tag{3.14}$$

where H_{1k} denotes the value of the Hamiltonian $\hat{H}_1$ at x_k.

The propagation of the wave function with respect to H_2 is performed using the semi-implicit Crank-Nicolson (CN) scheme, which discretizes Eq. (3.13) as follows

$$i\,\frac{\Psi_k^{n+1} - \Psi_k^{n+1/2}}{\triangle t} = H_2\,\frac{\Psi_k^{n+1} + \Psi_k^{n+1/2}}{2}. \tag{3.15}$$

The time derivative is approximated as a difference between the wave function value at the end of the propagation and its current value, divided by the step size. On the right-hand side, the operator $\hat{H}_2$ acts on a wave function written in a semi-implicit form, i.e., a linear combination of its current value and value at the end of propagation. It would be much simpler to use an explicit algorithm, where we have just the current value of the wave function on the right-hand side, but the semi-implicit scheme is absolutely stable, which makes it the preferred choice.

Numerically, the second derivative of a function $f(x)$ is approximated by taking the Taylor expansion of $f(x+h)$ and $f(x-h)$ to the order of h^2 (where h is a small quantity), and summing up these two expressions. This gives the following three-point formula for the second derivative

$$\frac{d^2 f(x)}{dx^2} = \frac{f(x-h) - 2f(x) + f(x+h)}{h^2} + O(h^2). \tag{3.16}$$

Using this relation, Eq. (3.15) can be written as

$$i\,\frac{\Psi_k^{n+1} - \Psi_k^{n+1/2}}{\triangle t} = \frac{-\Psi_{k-1}^{n+1} + 2\Psi_k^{n+1} - \Psi_{k+1}^{n+1} - \Psi_{k-1}^{n+1/2} + 2\Psi_k^{n+1/2} - \Psi_{k+1}^{n+1/2}}{2h^2}. \tag{3.17}$$

In this equation, the intermediate values of the wave function $\Psi^{n+1/2}$ are known at all points in space, and the values of the wave function Ψ^{n+1} at time t_{n+1} are to be calculated. By grouping all the coefficients in front of the unknown terms, Eq. (3.17) can be expressed in the following form

$$A_-\Psi_{k-1}^{n+1} + A_0\Psi_k^{n+1} + A_+\Psi_{k+1}^{n+1} = B_k, \tag{3.18}$$

where the coefficients are

$$\begin{aligned} A_0 &= 1 + i\,\frac{\triangle t}{h^2}, \\ A_- &= A_+ = -\,i\,\frac{\triangle t}{2h^2} \equiv A_\pm, \\ B_k &= \Psi_k^{n+1/2} + i\,\frac{\triangle t}{2h^2}\left(\Psi_{k-1}^{n+1/2} - 2\Psi_k^{n+1/2} + \Psi_{k+1}^{n+1/2}\right). \end{aligned} \tag{3.19}$$

The coefficients $A_\pm$ and A_0 are independent on the space and time coordinate, while the coefficient B_k contains all information about the calculated intermediate value of the wave function, and is dependent on the grid point and time (implicitly, through wave function values).

We assume that the solution for the wave function can be expressed in a recursive form

$$\Psi_{k+1}^{n+1} = \alpha_k \Psi_k^{n+1} + \beta_k. \tag{3.20}$$

By inserting this relation into Eq. (3.18), we obtain the equation

$$\left(A_0 + A_\pm \alpha_k\right) \Psi_k^{n+1} + A_\pm \Psi_{k-1}^{n+1} = B_k - A_\pm \beta_k. \tag{3.21}$$

This is the same relation between Ψ_k^{n+1} and Ψ_{k-1}^{n+1} as 3.20, so we deduce that the values of the coefficients α_k and β_k are given by

$$\begin{aligned} \alpha_k &= -\frac{A_\pm}{A_0 + A_\pm \alpha_{k+1}}, \\ \beta_k &= \frac{B_{k+1} - A_\pm \beta_{k+1}}{A_0 + A_\pm \alpha_{k+1}}. \end{aligned} \tag{3.22}$$

This is a recursive relation for coefficients; α_k and β_k depend on the values α_{k+1} and β_{k+1}, thus we need to set the boundary conditions in order to be able to calculate them. Since the value of the wave function at the simulation box border is set to zero, the coefficients α_{N_x-2} and β_{N_x-2} must be also equal to zero. In this way, going recursively backwards on the grid, the values of these coefficients can be obtained at all grid points. Having calculated that, and using the fact that the value of the wave function at the other boundary Ψ_0^{n+1} is also zero, by going recursively forward on the grid, we calculate the values of the wave function at all grid points, using Eq. (3.20).

To summarize, to calculate the wave function at time step $n+1$, we first propagate the wave function at time step n with respect to $\hat{H}_1$ to obtain the intermediate solution, which comes down to multiplying the wave function at each grid point by a factor determined by the trap potential value and interaction terms. This intermediate solution of the wave function is then used to calculate the coefficients α_k and β_k by backward sweep of the spatial grid, and those coefficients are subsequently used in a forward sweep of the spatial grid to determine the wave function at time step $n+1$. This procedure is then repeated until the end of the time propagation.

3.2.1 Generalization to the dipolar GP equation in 3D

Generalization to the 3D case is straightforward, since the derivatives along different axes commute with each other, and can be performed in a split-step fashion, as we have already seen. The space is now discretized along each direction, making the 3D space grid of size $N_x \times N_y \times N_z$. The complete propagation from t_n to t_{n+1} is now performed in four substeps, with respect to four parts of the Hamiltonian given below (for simplicity,

from now on we omit the tilde signs):

$$\hat{H}_1 = \eta^2(\rho - R)^2 + \lambda^2 z^2 + gn(\boldsymbol{r}, t) + g_{\mathrm{dd}} \int d\boldsymbol{r}'\, V_{\mathrm{dd}}(\boldsymbol{r} - \boldsymbol{r}')n(\boldsymbol{r}', t) + \Delta\mu(\boldsymbol{r}, t),$$
$$\hat{H}_2 = -\frac{\partial^2}{\partial x^2}, \quad \hat{H}_3 = -\frac{\partial^2}{\partial y^2}, \quad \hat{H}_4 = -\frac{\partial^2}{\partial z^2}. \tag{3.23}$$

As in 1D, the propagation is first performed with respect to $\hat{H}_1$, and then with respect to $\hat{H}_2$, $\hat{H}_3$ and $\hat{H}_4$, in arbitrary order.

When it comes to the first, non-derivative part of the Hamiltonian, we note several important points. First, while describing the CN method in the previous section, we did not mention that $\hat{H}_1$ depends on the wave function itself. Since we cannot solve the equation in an exact, self-consistent way, we have to solve it iteratively. The wave function at time step n is used to calculate the Hamiltonian $\hat{H}_1$, which is then used to produce the intermediate values of the wave function.

The second point is that calculation of the dipole-dipole term is quite time consuming, since it involves the integration over the entire space that needs to be performed at each time step. This can be partially mitigated using the Fourier transformation, which can be performed much faster by a library call to the appropriate FFTW function [38]. Namely, the DDI term is a convolution of two functions, and can be calculated as inverse Fourier transform of the product of their Fourier transforms,

$$\int d\boldsymbol{r}'\, V_{\mathrm{dd}}(\boldsymbol{r} - \boldsymbol{r}')n(\boldsymbol{r}', t) = \mathcal{F}^{-1}\Big[\mathcal{F}\big[V_{\mathrm{dd}}\big] \cdot \mathcal{F}\big[n\big]\Big]. \tag{3.24}$$

The Fourier transform of the dipole-dipole potential does not depend on time, and can be calculated exactly:

$$\mathcal{F}\big[V_{\mathrm{dd}}\big](\mathbf{k}) = \frac{4\pi}{3}\left(3\cos^2\theta - 1\right), \tag{3.25}$$

where $\cos\theta = k_z/|\mathbf{k}|$.

3.3 Calculation of the ground state

The method described in the previous section enables the computation of system's dynamics starting from some known initial state. However, the same method can be used to calculate the ground state of the system, if applied in imaginary time, $t \to -it$, which corresponds to Wick rotation. The method is therefore called the *imaginary-time propagation*. We stress that this method is purely mathematical and does not correspond to physical time propagation. In other words, it simply projects the given initial state to the ground state of the system. Since propagation in imaginary time does not preserve the norm of the wave function (the evolution operator is not unitary), note that it has to be renormalized in each time step.

The reasoning behind this method is as follows. The arbitrary state $\Psi(\boldsymbol{r})$ can be represented as a linear combination of the eigenstates, which are solutions to the eigenproblem $\hat{H}\phi_k(\boldsymbol{r}) = E_k\phi_k(\boldsymbol{r})$,

$$\Psi(\boldsymbol{r}) = \sum_k c_k\,\phi_k(\boldsymbol{r}). \tag{3.26}$$

The coefficients c_k are determined by projections of the wave function Ψ onto the eigenspaces spanned by the states ϕ_k. Let us denote by ϕ_0 the ground state of the system, i.e., the lowest energy state. The imaginary-time evolution of Ψ, that is, a solution to the time-dependent Schrödinger equation

$$-\frac{\partial\Psi(\boldsymbol{r},t)}{\partial t} = \hat{H}\Psi(\boldsymbol{r},t) \tag{3.27}$$

is given as follows

$$\Psi(\boldsymbol{r},t) = \sum_k c_k\,\phi_k(\boldsymbol{r})\,e^{-E_kt/\hbar}. \tag{3.28}$$

We can extract the "phase" factor $e^{-E_0t/\hbar}$ of the lowest energy state in front of the sum, to obtain the following expression

$$\Psi(\boldsymbol{r},t) = e^{-E_0t/\hbar}\left(c_0\phi_0 + \sum_{k>0} c_k\phi_k(\boldsymbol{r})\,e^{-(E_k-E_0)t/\hbar}\right). \tag{3.29}$$

The quantity $E_k - E_0$ is always greater than zero for $k > 0$ since E_0 corresponds to the lowest energy state. In imaginary-time propagation all terms for $k > 0$ exponentially decay due to exponential factors $e^{-(E_k-E_0)t/\hbar}$ in the above sum, and will go to zero in the long-time limit. Therefore, after a sufficiently long propagation time, only the term proportional to ϕ_0 will remain. Since the norm of the wave function is not preserved, and it needs to be normalized to unity after each time step, this will eliminate the coefficient in front of ϕ_0 (which is normalized), thus yielding only the ground state in the long-time limit. In practice, the propagation is performed until a convergence is achieved, which can be monitored by calculating the energy of the system, or relevant expectation values.

In this way, the ground state of the system, i.e., the solution of the time-independent GP equation (2.21), can be obtained using the same numerical method as for calculation of the system's dynamics, just by switching to imaginary time and renormalizing the wave function in each time step. This comes down to replacing the factor $i\triangle t$ in equations (3.14) and (3.19) with $\triangle t$. Usually, the initial state for the imaginary-time propagation is taken to be a Gaussian with parameters corresponding to the trap frequencies (i.e. the solution in the case of a non-interacting gas). The resulting ground state, or its small perturbation, is taken as an initial state for the real-time propagation of the system, in order to observe its low-temperature characteristics.

3.4 Calculation of relevant physical quantities

In order to study properties of the system and their dynamics, we need to calculate relevant physical quantities using the wave function at a given time t. The most useful

quantities are the condensate density, chemical potential, and expectation value of the system size.

The condensate density is calculated simply by taking the modulus squared of the wave function,

$$n(\boldsymbol{r},t) = |\Psi(\boldsymbol{r},t)|^2 . \tag{3.30}$$

Since it is difficult to visualize the three-dimensional density, the relevant two- and one-dimensional projections can be defined by integrating $n(\boldsymbol{r},t)$ over some coordinates, for instance

$$n_{2D}(x,y,t) = \int_{\mathbb{R}} dz\ |\Psi(\boldsymbol{r},t)|^2 , \quad n_{1D}(z,t) = \int_{\mathbb{R}^2} dx\,dy\ |\Psi(\boldsymbol{r},t)|^2 . \tag{3.31}$$

All densities and density projections calculated in this way are dimensionless, and can be converted to physical units by multiplying with the appropriate unit (l^{-3} in 3D, l^{-2} in 2D, and l^{-1} in 1D).

The chemical potential can be defined only for stationary states, where it represents the eigenvalue of the Hamiltonian in the ground state. It is calculated as $\mu = \mu_0 + \Delta\mu$, where μ_0 is the chemical potential of the case when quantum fluctuations are not taken into account, and $\Delta\mu$ represents the contribution due to this effect. The value of $\Delta\mu$ is easily calculated if the density of the wave function is known, according to Eq. (3.6). To calculate μ_0, we need to start from the dimensionless time-independent Gross-Pitaevskii equation,

$$\mu_0\Psi(\boldsymbol{r}) = \left[-\Delta + U(\boldsymbol{r}) + g\,|\Psi(\boldsymbol{r})|^2 + g_{\mathrm{dd}} \int d\boldsymbol{r}'\, V_{\mathrm{dd}}(\boldsymbol{r}-\boldsymbol{r}')\,|\Psi(\boldsymbol{r})|^2 \right] \Psi(\boldsymbol{r}). \tag{3.32}$$

We multiply this equation by $\Psi^*(\boldsymbol{r})$ from the left-hand side, and integrate over the entire space to obtain the value for μ_0. The total chemical potential is then given by the following equation

$$\begin{aligned} \mu = \int d\boldsymbol{r} \Bigg[& |\nabla\Psi(\boldsymbol{r})|^2 + (\gamma^2x^2 + \nu^2y^2 + \lambda^2z^2)\,|\Psi(\boldsymbol{r})|^2 + g\,|\Psi(\boldsymbol{r})|^4 \\ & + g_{\mathrm{dd}} \int d\boldsymbol{r}'\, V_{\mathrm{dd}}(\boldsymbol{r}-\boldsymbol{r}')\,|\Psi(\boldsymbol{r}')|^2\,|\Psi(\boldsymbol{r})|^2 \Bigg] + \frac{32}{3} g \sqrt{\frac{Na_s}{\pi}}\, Q_5(\epsilon_{\mathrm{dd}})\ |\Psi(\boldsymbol{r})|^3 . \end{aligned} \tag{3.33}$$

The dimensionless quantity μ can be expressed in physical units by multiplying with $\hbar\omega_{\mathrm{ref}}$. Even though the chemical potential is defined and physically relevant only for stationary states, we generalize the above definition and calculate it during the time propagation when it represents just the expectation value of the Hamiltonian, i.e., the energy of the system. For example, the convergence of the chemical potential in imaginary-time propagation is used as a criterion for the convergence of the wave function to the ground state. Similarly, in real-time propagation we expect the chemical potential to remain constant if the initial state is stationary for the system. On the other hand, sudden

change of the chemical potential may indicate, for example, the transition of the system to a different, metastable state.

As a measure of the condensate size it is common to use the root-mean-square (RMS) value of the coordinates (since mean value is zero for even potentials):

$$x_{rms} = \sqrt{\langle x^2 \rangle}, \quad \langle x^2 \rangle = \int d\boldsymbol{r}\, x^2 \left|\Psi(\boldsymbol{r}, t)\right|^2, \tag{3.34}$$

and similarly for y and z. The size of the whole system is taken as a quadratic mean of the coordinate RMS values,

$$r_{rms} = \sqrt{\langle x^2 \rangle + \langle y^2 \rangle + \langle z^2 \rangle}. \tag{3.35}$$

All calculated RMS values of the coordinates are dimensionless, and are expressed in physical units by multiplying with l.

The above physical quantities are the output of numerical simulations and can be directly compared to experimental results. They are not routinely calculated in each time step, since that would be too computationally demanding. Instead, they are calculated periodically, after a given number of time steps.

Chapter 4

Results

Here we present results of a numerical study of the emergence and properties of quantum droplets in ring-shaped Bose-Einstein condensates of ^{164}Dy atoms [14, 15]. We consider the contact interaction quench scenario, as discussed in Sec. 2.5. The system is initially in its ground state, with parameters tuned such that the Bose-Einstein condensate phase is obtained. The dynamics of the system is initiated by a sudden quench of the s-wave scattering length, which may lead to instability and eventual emergence of droplets, depending on the quench size. However, the shape of the trap potential introduces here additional, geometric restrictions on the behavior of the system, equivalent to periodic boundary conditions along the ring. This configuration is not yet studied in the literature to the best of our knowledge, and we expect interesting features to appear due to system's topology.

4.1 System parameters

In this section we briefly give physical and numerical parameters used for calculation in this thesis. We consider the system made up of dysprosium ^{164}Dy atoms confined in a ring potential (3.1). This atomic species has a rather large magnetic dipole moment of about 10 μ_B, where μ_B stands for the Bohr magneton. As a consequence, the system exhibits significant dipolar effects and its properties strongly depend on the trap geometry and the orientation of the dipoles, which are assumed to be along z direction. The number of atoms in the condensate was varied from 10,000 to 150,000. The mass of ^{164}Dy is $m \approx 164\,u$, where u is the atomic mass unit. According to Eq. (2.24), the strength of the DDI is $a_{\mathrm{dd}} = 132\,a_0$, where a_0 is Bohr radius. The strength of the contact interaction is taken to be $a_s^{(0)} = 132\,a_0$ before the quench, and after the quench it was decreased to a value in the range from $a_s = 47\,a_0$ to $78\,a_0$.

The trap potential is defined by the frequencies ω_ρ and ω_z, which are taken to be equal to $2\pi \times 600$ Hz, and the ring radius is $R = 10\,\mu$m, consistent with [39]. Reference frequency used to obtain dimensionless form of all quantities is $\omega_{\mathrm{ref}} = \omega_\rho = \omega_z$, such that the trap aspect ratios are $\eta = \lambda = 1$.

The unit of length is $\ell = \sqrt{\hbar/(m\omega_{\rm ref})} = 0.3205\,\mu$m, and the unit of time is $\tau = 2/\omega_{\rm ref} = 0.5305$ ms. The simulation box consists of $N_x = N_y = 512$ and $N_z = 128$ grid points along the corresponding axes, each spaced by $h_x = h_y = h_z = 0.15\,\ell$.

In the imaginary-time propagation used to calculate the ground state, we use $N_{\rm iter} = 3,000$ iterations with the time step $\triangle t = 0.002\,\tau$, since the wave function has shown to converge well during the time $N_{\rm iter}\triangle t$. The real-time propagation is performed for $N_{iter} = 50,000$ iterations with the time step $\triangle t = 0.001\,\tau$, which corresponds to the physical time of $t = 26.5$ ms. The density distribution and other relevant quantities are typically saved every 200 iterations.

4.2 Ground state

The ground state of the system is calculated using the imaginary-time propagation technique described in Sec. 3.3. The initial state is selected in the form of a Gaussian ring,

$$\Psi_0 \propto e^{-\frac{1}{2}\left[\eta^2(\rho-R)^2+\lambda^2 z^2\right]}. \tag{4.1}$$

Figure 4.1 shows the dependence of the chemical potential and the root-mean-square (rms) coordinates during the imaginary-time propagation, for three different values of the total atom number. As we see, the convergence is reached very quickly, which reflects

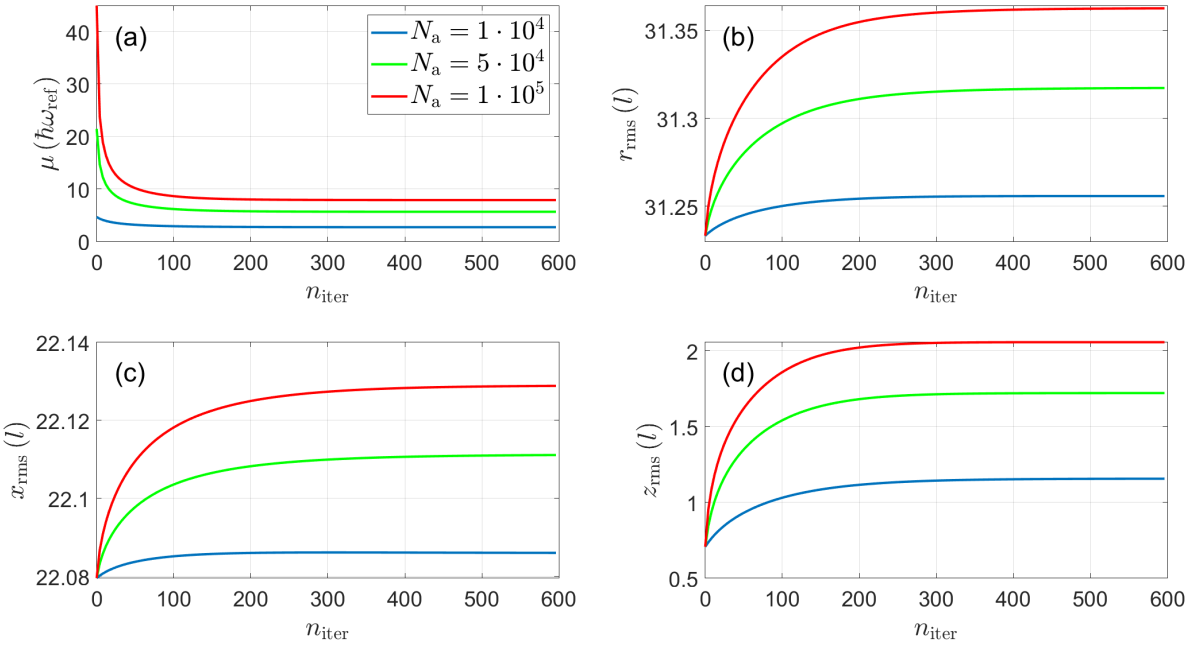

Figure 4.1: Imaginary-time dependence of relevant physical quantities: (a) chemical potential in units of $\hbar\omega_{\rm ref}$, (b) size of the system defined by Eq. (3.35), and the rms of coordinates (c) x and (d) z in units of ℓ. The total atom number is $N_{\rm a} = 10,000$ (blue), $N_{\rm a} = 50,000$ (green), and $N_{\rm a} = 100,000$ (red).

the fact that the initial wave function is a reasonably good approximation of the exact solution. However, the propagation is executed for a total of $N_{\text{iter}} = 3,000$ iterations to obtain high numerical precision of the ground state wave function, necessary for the real-time evolution of the system after the quench of the contact interaction. The rms of coordinate y is not plotted, since the system is cylindrically symmetric.

As expected, we see from Fig. 4.1(a) that increase in the number of atoms yields increase in the chemical potential of the ground state. We also see from Figs. 4.1(c) and 4.1(d) that the system size in z direction z_{rms} is significantly smaller than the corresponding sizes $x_{\text{rms}} = y_{\text{rms}}$. The size of the whole system r_{rms} converges to a value that is in a range from 31.25 to 31.36, which corresponds to the ring radius expressed in dimensionless units, $R = 31.20$. The quantity z_{rms} is in fact associated with the width of the ring, while x_{rms} is associated with its radius. Since the width of the ring is much smaller than its radius, it is effectively a 1D problem with periodic boundary conditions. As a consequence, the choice of parameters for such a system must be carefully made, so that the spatial grid is large enough to enclose the whole ring, but at the same time, to have the spacing small enough so as to properly capture the dynamics on the ring with sufficiently high accuracy. A shape of a typical ground state is shown in Fig. 4.3(a).

4.3 Droplet formation

As discussed in Sec. 2.5, quantum droplets can be formed starting from a ground state in a BEC phase, by performing a sudden quench of the contact interaction strength. We model this experimental protocol and numerically simulate real-time evolution of the system. Note that the system is not in the ground state after the quench, and therefore we cannot use the imaginary-time propagation to calculate the corresponding states obtained in current experiments. However, if experiments become able to realize ground states of dropletized systems, the numerically direct way to obtain them would be to use imaginary-time propagation.

We now study the behavior of quantum droplets for different values of the contact interaction strength a_{s}, different numbers of atoms N_{a}, while the DDI strength is kept at

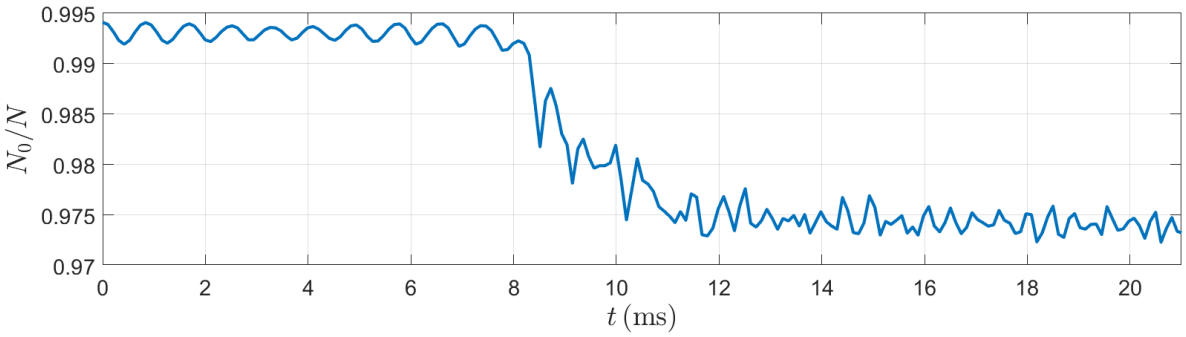

Figure 4.2: Time dependence of the condensate fraction after the contact interaction quench $a_s = 132\,a_0 \longrightarrow 45\,a_0$, for $N_{\text{a}} = 10,000$ atoms.

fixed value $a_{\mathrm{dd}} = 132a_0$.

Figure 4.2 shows the fraction of particles in the condensate as a function of time after the quench $a_s = 132a_0 \longrightarrow 45a_0$, for $N_{\mathrm{a}} = 10,000$ particles. We observe that the condensate depletion $\Delta N = 1 - N_0/N$ is less than one percent at the beginning of the propagation, but at some point it starts to increase and after the emergence of droplets has a value of of 2-3 %. That this increase in the condensate depletion corresponds to the process of droplet creation can be confirmed by examining the density of the system. Figure 4.3 shows a two-dimensional density distribution $n_{2\mathrm{D}}$ in the xy plane at characteristic times. We start from a condensate in a BEC phase, in its ground state shown in Fig. 4.3(a), to which a quench in the contact interaction strength is applied. After approximately $t = 8\,\mathrm{ms}$ clustering of particles occurs at some points along the ring, which is demonstrated in Fig. 4.3(b). This time corresponds to the beginning of

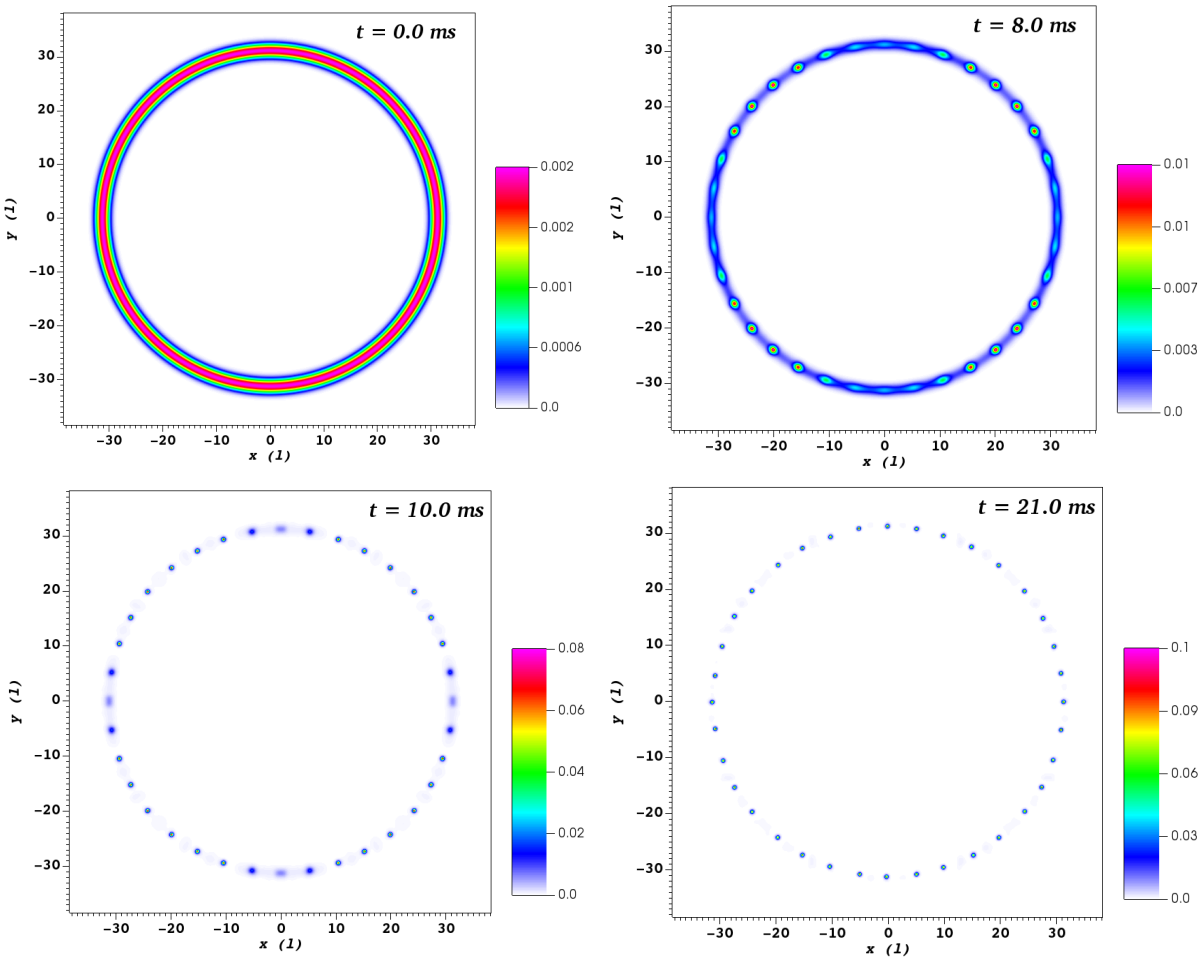

Figure 4.3: Density distribution plots at different times after the contact interaction quench for $N_{\mathrm{a}} = 10,000$ atoms. (a) The system is initially in a BEC phase in its ground state, when the contact interaction quench $a_s = 132\,a_0 \longrightarrow 45\,a_0$ is applied. (b) The beginning of particle rearrangement. (c) Droplets start to form and exchange atoms between each other. (d) The system is in a stable dropletized state.

a decrease in the condensate fraction, as can be seen from Fig 4.2. After some further evolution time distinct droplets are formed, as seen in Fig. 4.3(c). Except for a small particle exchange between droplets, they are stable until the end of propagation, shown in Fig 4.3(d). The same happens to the number of particles in the condensate, which converges to a certain value, around which it oscillates after the droplets are fully formed.

4.4 Critical strength of the contact interaction

We now determine a critical (maximal) value of the contact interaction strength after the quench a_s^{c}, such that the droplets do not form if a_s is quenched to a higher value than a_s^{c}. For a fixed number of atoms N_{a}, this is done by varying the value of a_{s} with the step of a_0, and examining the density plots to observe when the droplets start to emerge. The propagation is done for 50,000 iterations, which corresponds to 26.3 ms. The number of atoms is varied from 10,000 to 150,000 in order to measure the dependence of a_s^{c} on N_{a}.

For low atom numbers, the transition to a dropletized state is quite clear, as we have

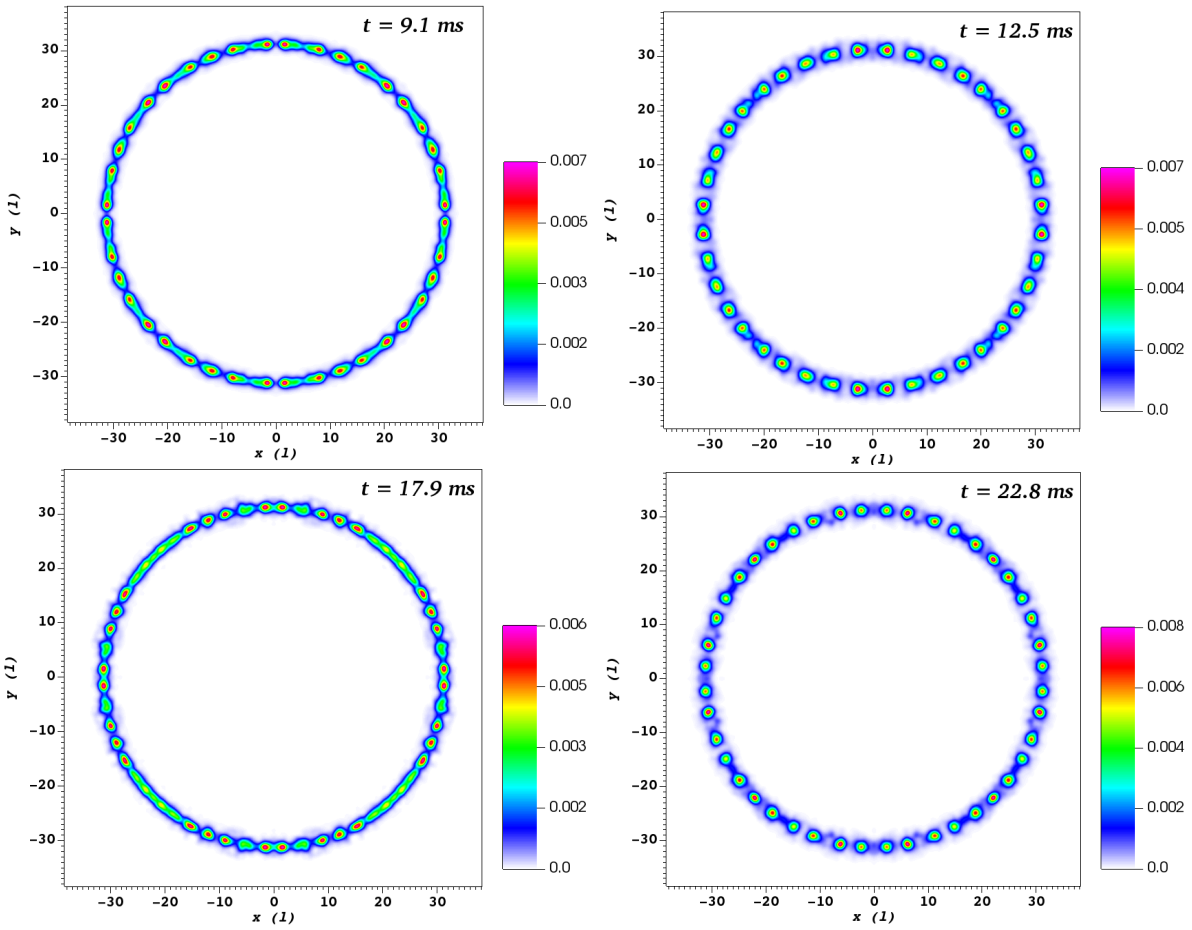

Figure 4.4: Density distribution plots at different propagation times in real-time system's dynamics for $N_{\mathrm{a}} = 80,000$ particles, and a quench in the contact interaction $a_s = 132\,a_0 \longrightarrow 77\,a_0$.

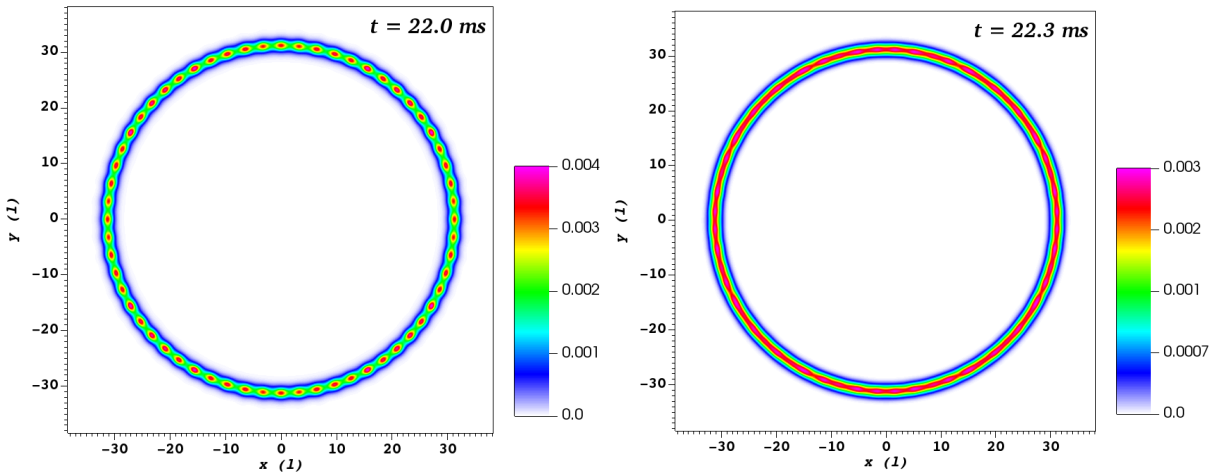

Figure 4.5: Density distribution plots at different propagation times in real-time system's dynamics for $N_{\rm a} = 50,000$ particles, and a quench in the contact interaction $a_s = 132\,a_0 \longrightarrow 76\,a_0$. The system oscillates between states presented in the left and in the right panel.

seen in Fig. 4.3. After formation, the droplets remain stable during propagation, and their number does not change. However, for higher numbers of atoms, and for values of $a_{\rm s}$ close to the phase transition, it is not always clear by just looking at the density plots weather the transition has happened or not. Figure 4.4 shows one such case, for $N_{\rm a} = 80,000$ and $a_{\rm s}$ quenched from $a_s^{(0)}$ to $a_s = 77\,a_0$. A number of droplets is indeed formed after about 9 ms, but the whole system is clearly not dropletized. During the time evolution the droplets form and disappear, their number is changing, and there is a substantial exchange of atoms between the droplets.

If a quench is performed to a somewhat higher value of $a_{\rm s}$, the system may end up in a state representing a transition between the dropletized and the BEC state. An example of this is given in Fig. 4.5. Regions of high density arise (left) and disappear (right), and the system oscillates between these two states, but it never produces isolated droplets. If the quench is made to even higher value of a_s, the system remains in the BEC phase, and no qualitative changes are observed during the dynamics. Of course, the quench excites all kinds of collective modes, which can be quantitatively observed.

In order to characterize the emergence of droplets, we consider the condensate density along the ring and assume that if one droplet is formed (i.e., if there is an 'opening' of the wave function on the ring, a region where the density vanishes), the system will eventually reach a fully dropletized state, after a sufficiently long evolution time. Since our computational resources are limited, we adopt the following numerical criterion, based on the analyzed data from extensive simulations we performed. First, from the full 3D wave function we extract a 1D array with the values of the condensate density along the ring potential minimum:

$$n_{\rm 2D}(R,t) \equiv n_{\rm 2D}(x,y;t), \quad \text{where } x^2 + y^2 = R^2. \tag{4.2}$$

Periodically during the time evolution we calculate a ratio of the maximal and minimal

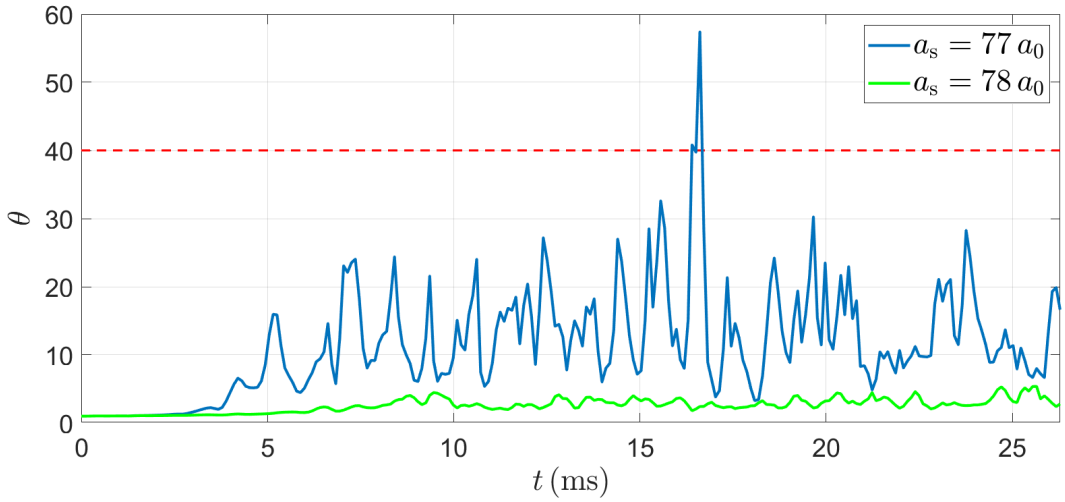

Figure 4.6: Time dependence of the ratio θ for $N_a = 80,000$ particles, and a contact interaction quench from $a_s = 132\,a_0$ to $77\,a_0$ (blue), and $78\,a_0$ (green). The dashed red line represents the critical value $\theta^c = 40$.

value of the density in the density array:

$$\theta(t) = \frac{\max\{n_{2D}(R,t)\}}{\min\{n_{2D}(R,t)\}}. \tag{4.3}$$

If this ratio is sufficiently high, we consider that the system reached a droplet-like state. The appropriate limit value for the quantity θ is determined by visually comparing the

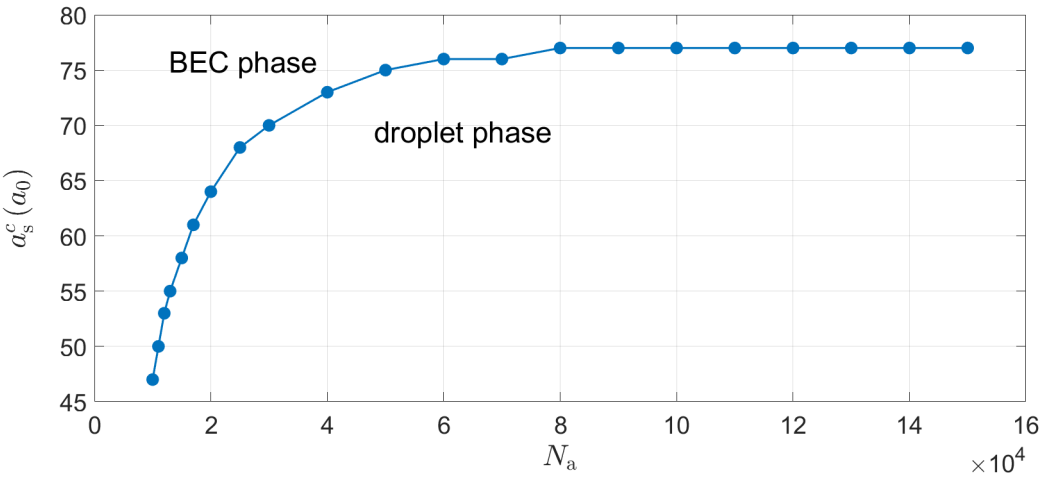

Figure 4.7: Phase diagram for the formation of quantum droplets: critical value of a_s^c, to which the system needs to be quenched in order to produce the droplets, as a function of the total number of atoms. The blue line that connects the numerically obtained points represents a transition line between the BEC phase and the droplet phase.

density plots with the corresponding ratio values, and in our analysis it is taken to be $\theta^{\rm c} = 40$. An example of the time dependence of θ for two close values of $a_{\rm s}$ is given in Fig. 4.6. For $a_s = 77\,a_0$, which corresponds to the density profiles shown in Fig. 4.4, we see that $\theta > \theta^{\rm c}$ at around $t = 16.6$ ms, and the droplets are expected to emerge. In order to have a fully dropletized state, $\theta(t)$ needs to exceed $\theta^{\rm c}$ frequently, or all the time.

Finally, in Fig. 4.7 we present the phase diagram in the plane $(N_{\rm a}, a_s^{\rm c})$ and denote regions corresponding to a BEC or a droplet state after the quench. The critical scattering length $a_s^{\rm c}$ rapidly decreases with the decrease of the number of atoms, but saturates to a value of around $a_s^{\rm c} = 77\,a_0$ for large $N_{\rm a}$. Note that we have not explored the region of small values of a_s, where the system may collapse instead of being dropletized. Therefore, Fig. 4.7 only indicated the upper bound for the droplet phase.

4.5 The number of droplets

Now that we have the phase diagram of the system and characterized its phases, we study in more detail the droplet phase, namely, how the number of droplets depends on the contact interaction strength for a fixed value of the atom number, and vice versa.

When a value of the contact interaction strength is fixed, we expect that, as we add more atoms, new droplets would emerge one by one. However, we observed that a

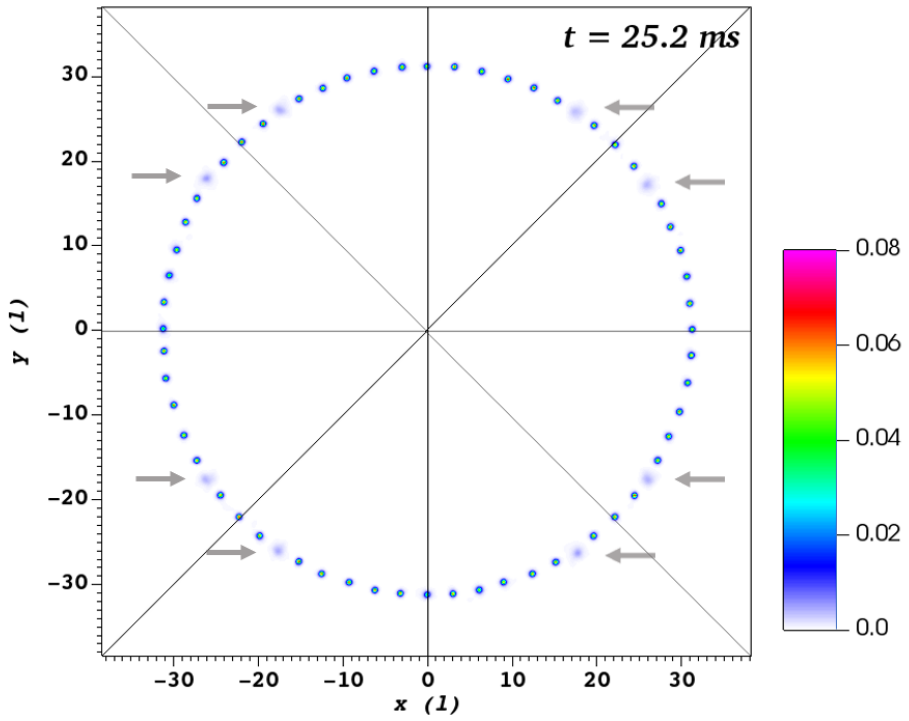

Figure 4.8: Density distribution plot in real-time system's dynamics for $N_a = 20,000$ particles, and a quench in the contact interaction $a_s = 132\,a_0 \longrightarrow 47\,a_0$. Arrows indicate the positions of eight fainter droplets, symmetrically distributed with respect to the shown axes.

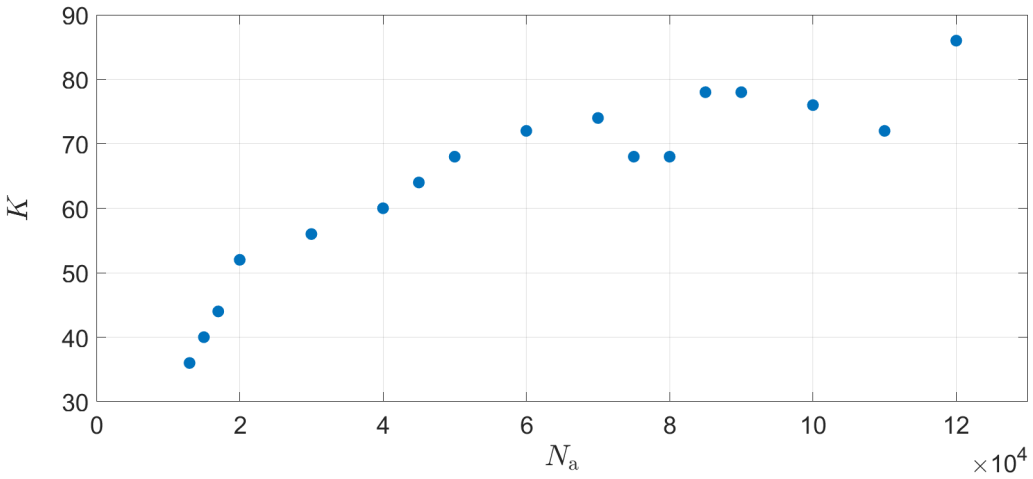

Figure 4.9: The number of droplets observed in the system's dynamics versus the total number of atoms, for a quench in the contact interaction $a_s = 132\,a_0 \longrightarrow 55\,a_0$.

number of droplets always changes in steps of 8. Moreover, we observe the corresponding symmetry in the density distribution, as can be seen in Fig. 4.8. Eight fainter droplets, denoted by arrows in the figure, are distributed symmetrically with respect to horizontal, vertical, and diagonal axes. We stress that there is no such discrete symmetry in the system, hence we conclude that it must be a byproduct of our numerical algorithm. To demonstrate this, we disrupt the artificial symmetry imposed by the Cartesian space grid in xy plane by changing the spacing in x and y direction to slightly different values: $h_x = 0.145$, $h_y = 0.155$. After introducing this spatial grid modification, previously observed discrete symmetry is reduced and there are only two or four fainter droplets. Further, by introducing a small noise to the ground state, which is always present in experiments, the artificial discrete symmetry is completely removed.

Figure 4.9 shows the dependence of the number of droplets K as a function of the particle number, for a fixed value of $a_s = 55$. We selected this value of a_s in order to be able to span a wide range of particle numbers, since it has to be smaller than the critical value, as determined from Fig. 4.7. We see that K increases with N_a, but the signal is not that clear and determining the obtained number of droplets is not easy in some cases. Therefore, there is an error associated with estimating the value of K of around 2, which has to be taken into account when interpreting the results from Fig. 4.9. Note that large numbers of atoms lead to increasingly large droplet numbers, which for $N \geq 90,000$ start to be placed not at the ring potential minimum line, but slightly off, in order to minimize the energy of the system. This further complicates the estimation of the droplet number, and therefore we do not show the results for $N \geq 120,000$ in Fig. 4.9.

Figure 4.10 shows the complementary dependence of the number of droplets as a function of the contact interaction strength, for a fixed value of the atom number $N_a = 60,000$. Again, this number is chosen such that it allows a wide range of values of a_s in the droplet phase in Fig. 4.7. We see that the droplet number decreases with increasing

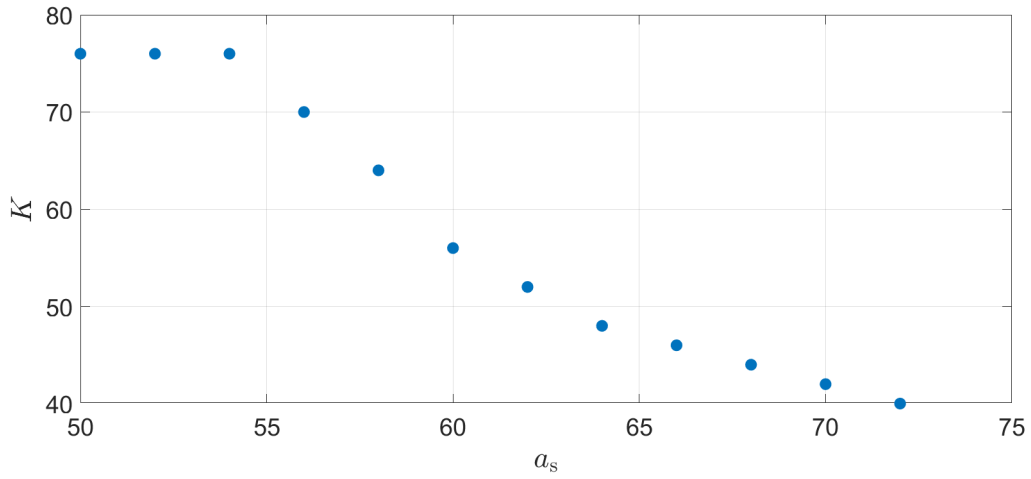

Figure 4.10: The number of droplets observed in the system's dynamics versus the contact interaction strength after the quench from $a_s^{(0)} = 132\,a_0$, for $N_a = 60,000$ particles.

a_s, but that it saturates for small values of a_s to around $N_a = 76$. For values of a_s higher than $72\,a_0$, the number of droplets cannot be clearly determined, since the system is then close to a transition to the BEC phase.

Chapter 5

Conclusions

In this thesis we studied the properties of dipolar Bose-Einstein condensates confined to a ring-shaped trap potential, in particular the emergence of quantum droplets due to a sudden quench of the contact interaction strength. Although such a system may exhibit a collapse at the mean-field level, if quantum fluctuations are taken into account the system may be stabilized. Furthermore, a new form of matter emerges, quantum droplets, as observed in recent experiments. We have provided a theoretical framework for the description of this phenomenon and numerically investigated the corresponding phase diagram. The obtained phase diagram determines the fate of the system as a function of the contact interaction quench size and the total number of atoms. We also determine the dependence of the number of droplets created after the quench as a function of the number of atoms and the quench size.

In the future we plan to study the transition between the BEC and the droplet phase, where a new, supersolid state may appear. While still superfluid, this state is also characterized by a spatial periodicity, i.e., a modulation of the density, and represents a set of quantum droplets that are closely connected such that the common wave function phase is preserved.

Chapter 6

References

Bibliography

[1] S. N. Bose, *Plancks gesetz und lichtquantenhypothese*, Z. Phys. **26**, 178 (1924).

[2] A. Einstein, *Quantentheorie des einatomigen idealen Gases*, Sitzungsber. Preuss. Akad. Wiss., Phys. Math. Kl. **22**, 261 (1924).

[3] P. Kapitza, *Viscosity of liquid helium below the λ-point*, Nature **141**, 74 (1938).

[4] J. F. Allen and D. Misener, *Flow of liquid helium II.*, Nature **141**, 75 (1938).

[5] F. London, *On the Bose-Einstein condensation*, Phys. Rev. **54**, 947 (1938).

[6] M. H. Anderson, J. R. Ensher, M. R. Matthews, C. E. Wieman, and E. A. Cornell, *Observation of Bose-Einstein condensation in a dilute atomic vapor*, Science **269**, 198 (1995).

[7] K. B. Davis, M. O. Mewes, M. R. Andrews, N. J. van Druten, D. S. Durfee, D. M. Kurn, and W. Ketterle, *Bose-Einstein condensation in a gas of sodium atoms*, Phys. Rev. Lett. **75**, 3969 (1995).

[8] C. C. Bradley, C. A. Sackett, J. J. Tollett, and R. G. Hulet, *Evidence of Bose-Einstein Condensation in an Atomic Gas with Attractive Interactions*, Phys. Rev. Lett. **75**, 1687 (1995).

[9] L. P. Pitaevskii and S. Stringari, *Bose-Einstein condensation*, Oxford University Press (2003).

[10] C. J. Pethick and H. Smith, *Bose–Einstein condensation in dilute gases*, Cambridge University Press (2008).

[11] T. D. Lee, K. Huang, and C. N. Yang, *Eigenvalues and eigenfunctions of a Bose system of hard spheres and its low-temperature properties*, Phys. Rev. **106**, 1135 (1957).

[12] N. Bogoliubov, *On the theory of superfluidity*, J. Phys. USSR **11**, 23 (1947).

[13] A. Griesmaier, J. Werner, S. Hensler, J. Stuhler, and T. Pfau, *Bose–Einstein condensation of chromium*, Phys. Rev. Lett. **94**, 160401 (2005).

[14] M. Lu, N. Q. Burdick, S. H. Youn, and B. L. Lev, *Strongly dipolar Bose-Einstein condensate of dysprosium*, Phys. Rev. Lett. **107**, 190401 (2011).

[15] Mingwu Lu, Seo Ho Youn, and Benjamin L. Lev, *Trapping ultracold dysprosium: a highly magnetic gas for dipolar physics*, Phys. Rev. Lett. **104** , 063001 (2010).

[16] K. Aikawa, A. Frisch, M. Mark, S. Baier, A. Rietzler, R. Grimm, and F. Ferlaino, *Bose-Einstein condensation of erbium*, Phys. Rev. Lett. **108** , 210401 (212).

[17] J. Stuhler, A. Griesmaier, T. Koch, M. Fattori, T. Pfau, S. Giovanazzi, P. Pedri, and L. Santos, *Observation of dipole-dipoleinteraction in a degenerate quantum gas*, Phys. Rev. Lett. **95**, 150406 (2005).

[18] T. Lahaye, C. Menotti, L. Santos, M. Lewenstein, and T. Pfau, *The physics of dipolar bosonic quantum gases*, Rep. Prog. Phys. **72**, 126401 (2009).

[19] S. Inouye, M. R. Andrews, J. Stenger, H. J. Miesner, D. M. Stamper-Kurn, and W. Ketterle, *Observation of Feshbach resonances in a Bose–Einstein condensate*, Nature **392**, 32354 (1998).

[20] J. Metz, T. Lahaye, B. Frohlich, A. Griesmaier, T. Pfau, H.Saito, Y. Kawaguchi, and M. Ueda, *Coherent collapse of a dipolar Bose-Einstein condensate for different trap geometries*, New J. Phys. **11**, 055032 (2009).

[21] H. Kadau, M. Schmitt, M. Wenzel, C. Wink, T. Maier, I. Ferrier-Barbut, and T. Pfau, *Observing the Rosensweig instability of a quantum ferrofluid*, Nature (London) **530**, 194 (2016).

[22] I. Ferrier-Barbut, H. Kadau, M. Schmitt, M. Wenzel, and T. Pfau, *Observation of quantum droplets in a strongly dipolar Bose gas*, Phys. Rev. Lett. **116**, 215301 (2016).

[23] M. Schmitt, M. Wenzel, F. Bottcher, I. Ferrier-Barbut, and T. Pfau, *Self-bound droplets of a dilute magnetic quantum liquid*, Nature (London) **539**, 259 (2016).

[24] I. Ferrier-Barbut, M. Schmitt, M. Wenzel, H. Kadau, and T. Pfau, *Liquid quantum droplets of ultracold magnetic atoms*, J. Phys. B **49**, 214004 (2016).

[25] Z. Luo, W. Pang, B. Liu, Y. Li, and B. A. Malomed, *A new form of liquid matter: quantum droplets*, arXiv (2020).

[26] B. A. Malomed, D. Mihalache, F. Wise, L. Torner, *Spatiotemporal optical solitons*, J. Optics B **7**, R53-R72 (2005).

[27] Abo-Shaeer, J and Raman, Chandra and Vogels, Johannes and Ketterle, W, *Observation of Vortex Lattices in Bose-Einstein Condensates*, Science (New York) **292** , 476 (2001).

[28] li, Junru and Lee, Jeongwon and Huang, Wujie and Burchesky, Sean and Shteynas, Boris and Top, Furkan and Jamison, Alan and Ketterle, Wolfgang *A stripe phase with supersolid properties in spin–orbit-coupled Bose–Einstein condensates*, Nature **543** , 91 (2017).

[29] P. Engels, C. Atherton, M. A. Hoefer, *Observation of Faraday waves in a Bose-Einstein condensate*, Phys. Rev. Lett. **98**, 095301 (2007).

[30] Castin, Y. *Bose-Einstein Condensates in Atomic Gases: Simple Theoretical Results*, Springer (2001).

[31] A. R. P. Lima and A. Pelster, *Quantum Fluctuations in Dipolar Bose Gases*, Phys. Rev. A **84** , 041604(R) (2011).

[32] A. R. P. Lima and A. Pelster, *Beyond Mean-Field Low-Lying Excitations of Dipolar Bose Gases*, Phys. Rev. A **86**, 063609 (2012).

[33] M. Wenzel, F. Bottcher, T. Langen, I. Ferrier-Barbut, and T. Pfau, *Striped states in a many-body system of tilted dipoles*, Phys. Rev. A **96**, 053630 (2017).

[34] C. Cabrera, L. Tanzi, J. Sanz, B. Naylor, P. Thomas, P. Cheiney, and L. Tarruell, *Quantum liquid droplets in a mixture of Bose-Einstein condensates*, Science **359**, 301 (2018).

[35] V. Loncar, L. E. Young-S., S. Skrbic, P. Muruganandam, S. K. Adhikari, and A. Balaz, *OpenMP, OpenMP/MPI, and CUDA/MPI C programs for solving the time-dependent dipolar Gross-Pitaevskii equation*, Comput. Phys. Commun. **209**, 190 (2016).

[36] V. Loncar, A. Balaz, A. Bogojevic, S. Skrbic, P. Muruganandam, and S. K. Adhikari, *CUDA programs for solving the time-dependent dipolar Gross–Pitaevskii equation in an anisotropic trap*, Comput. Phys. Commun. **200**, 406 (2016).

[37] R. K. Kumar, L. E. Young-S, D. Vudragovic, A. Balaz, P. Muruganandam, and S. K. Adhikari, *Fortran and C programs for the time-dependent dipolar Gross-Pitaevskii equation in an anisotropic trap*, Comput. Phys. Commun. **195** , 117 (2005).

[38] M. Frigo and S. G. Johnson, *FFTW – Fastest Fourier Transform in the West*, http://www.fftw.org/ (2016).

[39] S. Eckel, A. Kumar, T. Jacobson, I. B. Spielman, and G. K. Campbell, *A Rapidly Expanding Bose-Einstein Condensate: An Expanding Universe in the Lab*, Phys. Rev. X **8** , 021021 (2018).